Human DCP1 is crucial for mRNA decapping and possesses paralog-specific gene regulating functions

Ting-Wen Chen[1,2,3,7], Hsiao-Wei Liao[4,7], Michelle Noble[5], Jing-Yi Siao[6], and Chung-Te Chang[5,6,*]

[1]Institute of Bioinformatics and Systems Biology, National Yang Ming Chiao Tung University, Hsinchu 300, Taiwan
[2]Department of Biological Science and Technology, National Yang Ming Chiao Tung University, Hsinchu, 30068, Taiwan
[3]Center For Intelligent Drug Systems and Smart Bio-devices (IDS^{2}B), National Yang Ming Chiao Tung University, Hsinchu, Taiwan
[4]Department of Pharmacy, National Yang Ming Chiao Tung University, Taipei 112, Taiwan
[5]Department of Biochemistry, Max Planck Institute for Developmental Biology, Max-Planck-Ring 5, 72076 Tübingen, Germany
[6]Institute of Biochemistry and Molecular Biology, National Yang Ming Chiao Tung University, Taipei 112, Taiwan
[7]These authors contributed equally to this work.

* To whom correspondence should be addressed. Tel: +886 2 2826 7122; Fax: +886 2 2826 4843; Email: chungte.chang@nycu.edu.tw

ABSTRACT

The mRNA 5'-cap structure removal by the decapping enzyme DCP2 is a critical step in gene regulation. While DCP2 is the catalytic subunit in the decapping complex, its activity is strongly enhanced by multiple factors, particularly DCP1, which is the major activator in yeast. However, the precise role of DCP1 in metazoans has yet to be fully elucidated. Moreover, in humans, the specific biological functions of the two DCP1 paralogs, DCP1a and DCP1b, remain largely unknown. To investigate the role of human DCP1, we generated cell-lines that were deficient in DCP1a, DCP1b or both to evaluate the importance of DCP1 in the decapping machinery. Our results highlight the importance of human DCP1 in decapping process and show that the EVH1 domain of DCP1 enhances the mRNA-binding affinity of DCP2. Transcriptome and metabolome analyses outline the distinct functions of DCP1a and DCP1b in human cells, regulating specific endogenous mRNA targets and biological processes. Overall, our findings provide insights into the molecular mechanism of human DCP1 in mRNA decapping and shed light on the distinct functions of its paralogs.

INTRODUCTION

Gene expression must be stringently regulated to ensure efficient control of cellular processes. A key mechanism of gene expression regulation is the control of mRNA degradation (Chen and Shyu, 2017; Corbett, 2018), mediated by the removal of protective structures from mRNA, which suppresses translation or leads to mRNA degradation. In most eukaryotic cells, mRNA is stabilized through the addition during posttranscriptional modification of an N^7-methyl guanosine (m^7G) cap at the 5′ end and a polyA tail at the 3′ end (Furuichi et al., 1977; Garneau et al., 2007). General mRNA decay is typically initiated by deadenylation, which is mediated by the coordinated activity of the CCR4/NOT and PAN2/3 complexes (Chen and Shyu, 2011; Decker and Parker, 1993). Shortening of the polyA tail typically initiates mRNA decay, resulting in exonucleolytic degradation in the 5'-3' or 3'-5' direction, respectively facilitated by the exonuclease XRN1 or the exosome complex (Chang et al., 2019; Garneau *et al.*, 2007; Lim et al., 2016; Subtelny et al., 2014; Webster et al., 2018; Yi et al., 2018). While the cytoplasmic RNA exosome degrades mRNA in the 3'-5' direction, the primary effect of deadenylation is “mRNA decapping”, the removal of the m^7G cap structure at the 5'-end of the mRNA that otherwise prevents mRNA degradation (Stevens, 1988). This connection between deadenylation and decapping is facilitated by Pat1, which together with the Lsm1-7 complex, recruits the decapping complex through a combination of disordered and structured domains, promoting distinct steps of mRNA decay (Charenton et al., 2017; Charenton and Graille, 2018; Fourati et al., 2014; Lobel and Gross, 2020; Lobel et al., 2019; Sharif and Conti, 2013; Wu et al., 2014).

The mRNA decapping process is crucial for gene regulation because it leads to the irreversible removal of the mRNA cap structure, inhibiting translation initiation and inducing the XRN1-mediated degradation of mRNA through the 5′-3′ mRNA decay pathway (Hsu and Stevens, 1993; Topisirovic et al., 2011). Decapping does not only lead to the degradation of bulk mRNA molecules; it is also involved in specific mRNA decay pathways, such as AU-rich element-mediated decay, nonsense-mediated decay (NMD), and miRNA-triggered mRNA turnover (Arribas-Layton et al., 2013; Chen and Shyu, 2003; Fenger-Gron et al., 2005; Jonas and Izaurralde, 2015; Loh et al., 2013). Because of its crucial role in gene regulation, decapping is tightly regulated by the activity of both general and pathway-specific factors through various mechanisms. In the context of NMD for instance, target transcripts can be degraded through

endonucleolytic cleavage by SMG6 (Eberle et al., 2009; Huntzinger et al., 2008), or be facilitated by SMG5 in conjunction with the NMD effector SMG7 or the decapping factor PNRC2, leading to enhanced deadenylation and decapping (Cho et al., 2009; Fukuhara et al., 2005; Loh *et al.*, 2013). Understanding the determinants of the preferential associations between certain degradation mechanisms and particular transcripts requires further study (Metze et al., 2013). Overall, the pivotal role of decapping in the intricate network of mRNA decay justifies ongoing research in this field.

In eukaryotes, the removal of the mRNA 5′-m^7GDP cap structure is catalysed by the decapping enzyme DCP2, a pyrophosphatase belonging to the Nudix family of proteins. This process results in the generation of 5′ monophosphorylated mRNA, which is subsequently targeted for degradation (Arribas-Layton *et al.*, 2013; Lykke-Andersen, 2002; Steiger et al., 2003; van Dijk et al., 2002; Wang et al., 2002). The central component of the complex, DCP2, has two major domains: the N-terminal regulatory domain (NRD) and the catalytic Nudix domain (She et al., 2006; She et al., 2008). The positively charged patch of the Nudix domain plays a crucial role in RNA binding (Deshmukh et al., 2008; Piccirillo et al., 2003). Meanwhile, the NRD enhances decapping activity by specifically recognizing the m^7G nucleotide of the mRNA cap structure and interacts with the N-terminal EVH1 domain of the major activator DCP1, further accelerating the decapping process (Chang et al., 2014; Charenton et al., 2016; Dunckley and Parker, 1999; Floor et al., 2010; Mugridge et al., 2016; She *et al.*, 2008; Wang *et al.*, 2002; Wurm et al., 2017). Yeast Dcp2 has an additional unstructured C-terminal extension that contains short helical leucine-rich motifs (HLMs) responsible for protein-protein interactions and elements that inhibit Dcp2 catalytic activity (Charenton *et al.*, 2017; He and Jacobson, 2015). Interestingly, in contrast to yeast, metazoans have the HLM in DCP1, implying a conserved biological function with evolving regulation of mRNA decapping (Fromm et al., 2012).

Although DCP2 can exhibit catalytic activity on its own (Lykke-Andersen, 2002; van Dijk *et al.*, 2002; Wang *et al.*, 2002), it is important to note that additional cofactors are involved in stimulating DCP2 for complete activation. The primary activator of DCP2 in yeast is Dcp1, which is essential for decapping activity *in vivo* (Beelman et al., 1996) and considerably enhances the catalytic activity of Dcp2 *in vitro* (Deshmukh *et al.*, 2008; Floor *et al.*, 2010; She *et al.*, 2006). In addition to Dcp1, proteins such as Edc1-3, Pby1, Lsm1-7, Pat1, and Dhh1 (PNRC1,

PNRC2, EDC3, EDC4, Lsm1-7, Lsm14, PatL1, and DDX6 in metazoans) promote decapping by directly or indirectly interacting with Dcp2 (Charenton et al., 2020; Charenton *et al.*, 2017; Charenton and Graille, 2018; Charenton *et al.*, 2016; Cho *et al.*, 2009; Gaviraghi et al., 2018; He and Jacobson, 2022; He et al., 2022; Jonas and Izaurralde, 2013; Ling et al., 2011; Lobel *et al.*, 2019; Mugridge et al., 2018b). These proteins facilitate decapping through the assembly of messenger ribonucleoprotein (RNP) units or the structural rearrangement of DCP2. High levels of these proteins have been detected in large RNP granules, processing bodies (P-bodies), which likely serve as sites for the storage of translationally repressed RNAs and the process of mRNA decay (Eulalio et al., 2007; Jonas and Izaurralde, 2013; Luo et al., 2018).

The interactions between the subunits of the decapping complex are crucial for enhancing its activity and for the targeting of specific mRNAs. Although Dcp1 and Dcp2 have been shown to interact strongly in yeast, direct DCP1-DCP2 interactions are weak in metazoans. Instead, the metazoan-specific protein EDC4, which has binding sites for both DCP1 and DCP2, likely functions as a scaffold that brings these proteins together despite their weak interaction propensity (Chang *et al.*, 2014; Fenger-Gron *et al.*, 2005). In addition to EDC4, DCP1 acts as a binding platform for other coactivator proteins, such as yeast Edc1 and Edc2 and the human PNRC paralogs, PNRC1 and PNRC2 (Gaviraghi *et al.*, 2018; Jonas and Izaurralde, 2013; Mugridge *et al.*, 2016). In metazoans, the HLM domain of DCP1 interacts with the Lsm domains of proteins such as EDC3 and Lsm14 in a mutually exclusive manner. Moreover, in multicellular eukaryotes, DCP1 features a C-terminal extension that induces DCP1 trimerization, referred to as the trimerization domain (TD). Trimerization is a prerequisite for the incorporation of DCP1 into active decapping complexes and for promoting efficient mRNA decapping *in vivo* (Fromm *et al.*, 2012; Jonas and Izaurralde, 2013; Tritschler et al., 2007). This competition results in the formation of structurally and functionally distinct assemblies, contributing to target specificity (Vidya and Duchaine, 2022).

Recent structural analyses of the *Kluyveromyces lactis* Dcp1-Dcp2-Edc3 complex indicate that the Lsm domain of Edc3 binds to an extended helix at the C-terminus of the Dcp2 Nudix domain (Charenton *et al.*, 2016). Furthermore, the activation peptide of Edc1 bridges Dcp1 and Dcp2, as observed in the Edc1-Dcp1-Dcp2 complex in *Saccharomyces pombe* and *Kluyveromyces lactis* (Mugridge *et al.*, 2018b; Wurm *et al.*, 2017). These structural insights

suggest that Edc1 and Edc3 collaborate through distinct mechanisms, aiding the decapping process (Charenton and Graille, 2018; Charenton *et al.*, 2016; Mugridge et al., 2018a; Mugridge *et al.*, 2018b; Tibble et al., 2021). Specifically, Edc1 stabilizes Dcp2's catalytically active conformation, while Edc3 extends the RNA binding surface of the Dcp2 Nudix domain (Charenton *et al.*, 2016; Mugridge *et al.*, 2018b). This extended RNA interaction potentially accounts for the transcript-specific nature of Edc3-mediated decapping activation, hinting at distinct coactivators' roles in gene-specific regulation.

While structural studies suggest that interactions with Dcp1 are central to the activation of Dcp2 (Charenton and Graille, 2018; Deshmukh *et al.*, 2008; Mugridge *et al.*, 2018a; Mugridge *et al.*, 2016; She *et al.*, 2008; Valkov et al., 2016), the lack of structural information on the human decapping complex hinders our understanding of the specific role of human DCP1 in decapping. It remains unclear how DCP1 contributes to the conformational changes in the DCP2 catalytic cycle or to mRNA and cap structure recognition. A further complication is the existence of two paralogs of human DCP1, DCP1a and DCP1b, which have 31% sequence identity over their entire length (Lykke-Andersen, 2002; van Dijk *et al.*, 2002). The functional differences of these paralogs have yet to be determined. Studies of their potentially distinct roles in the decapping complex may provide new insight into the molecular mechanisms of mRNA decapping. The fact that decapping dysfunctions can have detrimental effects on cell growth and have been linked to severe neurological disorders in humans (Ahmed et al., 2015; Ng et al., 2015), highlights the importance of understanding the mechanisms of mRNA decapping regulation and the potential therapeutic implications.

In this study, we investigated the roles of human DCP1 in mRNA decapping by generating HEK-293T cell lines lacking DCP1a, DCP1b, or both. Our findings indicate that human DCP1 promotes decapping *in vivo* and that DCP1a and DCP1b play redundant roles in the general 5′-3′ mRNA decay pathway. We found that EVH1 domain may be crucial for enhancing DCP2's recruitment to target mRNA in cells. Multiomics analyses revealed distinct expressional and metabolomic profiles for the knockout cell lines. These results indicate that the DCP1 paralogs have distinct roles in the regulation of various biological processes. Overall, our findings offer valuable insights into the mechanisms underlying human DCP1-mediated mRNA decapping and the specific mRNA targets and biological processes regulated by DCP1a and DCP1b in humans.

MATERIAL AND METHODS

DNA constructs

The DNA constructs used in this study are listed in Supplementary Table 1. The plasmids for expression of the β-globin-6xMS2bs and the control β-globin-GAPDH (control) mRNAs were kindly provided by Dr. J. Lykke-Andersen and have been described previously (Lykke-Andersen et al., 2000).

CRISPR/Cas9-mediated gene editing

The HEK-293T DCP1a-, DCP1b-, and DCP1a/b-null cell lines were generated by CRISPR/Cas9-mediated gene editing as described previously (Sgromo et al., 2018). The guide RNA targeting human DCP1 paralog genes (DCP1a: GCTGTTTCGAGGTAAGCTGG; DCP1b: TCGGCCATCGGGCCAACGAG) was designed using the ATUM CRISPR gRNA Design tool. The absence of detectable levels of DCP1 protein was confirmed by Western blotting. Sanger sequencing of the targeted locus confirmed the presence of a deletion within the targeted exon resulting in a frameshift.

Tethering assays

Tethering assays using the MS2 reporter system were performed as described previously (Chang *et al.*, 2014). Briefly, HEK-293T cells were cultured in six-well plates and transiently transfected with a mixture of four plasmids: 0.5 µg control plasmid (β-globin-GAPDH), 0.5 µg plasmid encoding the β-globin-6xMS2bs, 0.5 µg plasmids encoding the MS2-tagged fusion protein (SMG7, TNRC6A-SD (silencing domain), or Nanos1) and plasmids encoding GFP-MBP, GFP-DCP2 E148Q, or GFP-DCP1 (wild-type or fragments) as indicated amounts. The cells were harvested two days after transfection. Total RNA was isolated using the TRIzol method (Thermo) and analysed by northern blot.

5’-phosphate-dependent exonuclease assay

The integrity of the 7-methylguanosine cap structure at the 5'-ends of the transcripts was investigated in a 5'-phosphate-dependent exonuclease assay. 10 μg RNA extracted from the specific tethering assays was incubated in a 20 μl reaction volume with 1 unit of Terminator 5'-phosphate-dependent exonuclease (Epicentre) for 60 min at 30°C. The Terminator was omitted in the control. The reaction was then stopped by adding phenol. After standard extraction and ethanol precipitation, RNA levels were visualized by northern blotting.

Immunofluorescence

Cells were fixed and permeabilized as described previously (Jakymiw et al., 2005). The antibodies used in this study are listed in **Supplementary Table 2**. The antibodies were diluted at 1:1000.

Decapping assays

Decapping assays were performed with immunoprecipitated wildtype GFP-DCP2 or a catalytic mutant (E148Q) from either wild-type DCP1a/b-null HEK-293T cells, along with in vitro-synthesized RNA (127 nucleotides) with a ^{32}P-labeled cap structure (Chang *et al.*, 2014). To generate the ^{32}P-labeled cap RNA, we utilized the ScriptCap m^{7}G Capping System and ScriptCap 2'-O-methyltransferase kit (Epicentre Biotechnologies) with [α-^{32}P] GTP for our experiments. The concentration of RNA used was 0.5 μM. The decapping reactions were performed at 30 °C for the indicated times in a total volume of 10 μl of decapping buffer (50 mM Tris-HCl (pH 7.5), 50 mM ammonium sulfate, 0.1% (w/v) BSA and 5 mM $MgCl_2$). The proteins were diluted to their working concentrations with the decapping buffer. The reactions were stopped by adding up to 50 mM EDTA (final concentration), and 1 μl of each sample was spotted on polyethylenimine (PEI) cellulose thin-layer chromatography plates (Merck) and developed in 0.75 m LiCl.

Co-immunoprecipitation assays and Western blot analysis

For immunoprecipitation assays, HEK-293T cells were seeded in 10 cm dishes and transfected with 20 μg total plasmid DNA using Lipofectamine 2000 (Thermo). The cells were washed 48 h after transfection with phosphate-buffered saline and lysed in 1 ml NET buffer (50 mM Tris-HCl (pH 7.5), 150 mM NaCl, 1 mM EDTA, 0.1% (v/v) Triton-X-100, 10% (v/v) glycerol and

supplemented with complete protease inhibitor cocktail (Sigma)). Immunoprecipitations were performed as described previously (Braun et al., 2012). RNase A (1 µl, 10 mg/ml) was added to the cell extract in all experiments. The antibodies used in this study are listed in Supplementary Table 2. All Western blots were developed with the ECL Western blotting analysis system (GE Healthcare) as recommended by the manufacturer.

PNRC1 and PNRC2 knockdown

Plasmids expressing short-hairpin RNAs (shRNAs) for knockdowns were derived from the pSUPER plasmid containing the puromycin-resistance gene for selection. The vector backbone was a kind gift from O. Mühlemann (University of Bern). The 19 nt target sequences were as follows: control: ATTCTCCGAACGTGTCACG, PNRC1: CAAAGTTTAGTGATCCACCTTT, and PNRC2: AGTTGGAATTCTAGCTTAT. HEK-293T cells were grown in DMEM supplemented with 10% heat inactivated fetal bovine serum and 2 mM L-Glutamine. The cells were transfected in 6-well plates using Lipofectamine 2000 (Thermo) according to the manufacturers' protocol. Transfection mixtures contained 0.5 µg control plasmid (β-globin-GAPDH), 0.5 µg plasmid encoding the β-globin-6xMS2bs, 0.5 µg plasmids encoding the MS2-tagged SMG7, and 2.5 µg of plasmids expressing the relevant shRNA. Twenty-four hours after transfection, cells were selected in medium supplemented with 1.5 µg/ml puromycin. After 24 h of selection, cells were counted and reseeded in new 6-well plates in medium without puromycin for recovery. After 24 h of reseeding, the cells were prepared for re-transfection to conduct tethering assays.

RNA immunoprecipitation assays

To perform RNA immunoprecipitation assays, HEK-293T DCP1a/b-null cells were cultured in 10 cm dishes and transiently transfected with a mixture of four plasmids: 5 µg of β-globin-6xMS2bs, 5 µg of plasmids encoding the MS2-HA-Strep-tagged SMG7, 5 µg of plasmids encoding V5-Streptavidin-Binding Peptide (SBP)-tagged DCP2 E148Q, and 5 µg of plasmids encoding GFP-MBP. Forty-eight hours after transfection, V5-SBP-DCP2 E148Q or MS2-HA-Strep-SMG7 was immunoprecipitated by Streptavidin (Thermo) or Strep-Tactin (IBA) beads, respectively, as described previously (Braun *et al.*, 2012).

The level of DCP2-bound reporter mRNA was extracted and reverse transcribed using b-globin reverse primer (TTAGTGATACTTGTGGGCCAGGGC). The amount of target mRNA was subsequently determined using quantitative PCR (qPCR) using the respective primer pair (Fw: ATGGTGCACCTGACTCCTGAG; Rev: TTAGTGATACTTGTGGGCCAGGGC). To use the Livak method (ΔΔCT method) for relative quantification, each primer pair was tested if the amplification rate of the specific PCR product was 2 ± 5%. To determine the level of DCP2 bound to reporter mRNA, Strep-tagged SMG7 was precipitated using Strep-Tactin beads, and the DCP2 level was detected by Western blot.

Transcriptome sequencing (RNA-Seq)

HEK-293T wild-type, DCP1a-, DCP1b-, or DCP1a/b-null cells were plated on 15 cm dishes 24 h before harvesting as described previously (Calviello et al., 2016). Total RNA was extracted using the RNeasy Mini Kit (Qiagen) and a library prepared using the TruSeq RNA Sample Prep Kit (Illumina). Three biological replicates were analysed. RNA-Seq libraries were sequenced using the Illumina NovaSeq 6000 sequencing system.

Metabolomics analysis (HILIC, LC–QToF)

LC-MS grade methanol and water were procured from Scharlau Chemie (Sentmenat, Barcelona, Spain) and MS-grade acetonitrile was obtained from J.T. Baker (Phillipsburg, NJ, USA). The remaining chemicals were purchased from MilliporeSigma (St. Louis, MO, USA), unless specified otherwise.

The number of cultured cells in each tube was adjusted to 10^6 in 100 µl PBS and quenched by using 400 µl of cold methanol. After centrifuging at 15000 xg for 5 min, the supernatant was collected and stored at -20 °C until use. Metabolomics data were acquired using an Agilent 1290 ultra-high-performance liquid chromatography (UHPLC) system (Agilent Technologies, Waldbronn, Germany) connected to a Bruker maXis ultra-high-resolution (UHR)-time-of-flight (TOF) mass spectrometer (Bruker Daltonics, Bremen, Germany). Metabolites were separated using a BEH Amide column (2.1 mm x 100 mm, 1.7 µm), with an injection volume of 10 µl. The autosampler and column temperatures were maintained at 4 and 40 °C, respectively. The mobile phase A consisted of 10 mM ammonium acetate in deionized water with 0.1% formic acid, and

the mobile phase B consisted of 10 mM ammonium acetate in a 5:95 (v/v) water:acetonitrile mixture with 0.1% formic acid. The flow rate was 0.4 mL min^{-1}. The elution gradient was as follows: 0–0.5 min, 99% mobile phase B; 0.5–7 min, 99%–50% mobile phase B; 7–10 min, 50% mobile phase B; and column re-equilibration with 99% mobile phase B for 2 min. The electrospray settings were: dry gas temperature, 200 °C; dry gas flow rate, 8 L min^{-1}; nebulizer gas pressure, 2 bar; capillary voltage, 4500 V; endplate offset potential, 500 V. Mass spectra were recorded over the range 50 to 1500 *m/z* in the positive mode. The TOF mass analyser was calibrated using sodium formate with a mass range of 50–1500 *m/z* before use.

The maXis UHR-TOF data were processed using MS-DIAL version 4.60 (accessible at http://prime.psc.riken.jp/) and Bruker Compass DataAnalysis version 4.1. For peak detection and alignment, the minimum peak height was set at an amplitude of 3000, the retention time tolerance was set at 0.1 min, and other parameters were set at their default values using the web-based metabolomics data processing tool MetaboAnalyst 5.0 (accessible at https://www.metaboanalyst.ca/). For statistical analysis, the data were normalized (mean-centred and divided by the standard deviation of each variable) and heat maps and volcano plots were constructed. Partial least squares discriminant analysis (PLS-DA) was performed using the R package, mixOmics (Rohart et al., 2017). Known features were first confirmed using a home-built compound library generated using commercial reference standards based on retention time and isotopic mass information. Unknown features of interest were further identified using the online databases METLIN (Guijas et al., 2018) and the Human Metabolome Database (Wishart et al., 2018).

Transcriptomics analysis

Transcriptomes were sequenced using high-throughput technology. Lo-quality bases and adapters were removed with Trimmomatic (Bolger et al., 2014). The filtered, high-quality reads were mapped to the human genome (GENCODE Human Release 33) and quantified with RSEM (Frankish et al., 2019; Li and Dewey, 2011). The TPM expression profiles from each sample were then used to generate PCA plots with R. The fold changes between different groups for each gene were estimated with DESeq2 (Love et al., 2014). Genes were defined as differentially expressed if the absolute value of the corresponding fold change was larger than 1.5 and the

adjusted p value was smaller than 0.05. Pathway analysis was performed using the clusterProfiler R package (Wu et al., 2021b); specifically, GSEA (Subramanian et al., 2005) was used to identify activated or suppressed GO terms (The Gene Ontology, 2019), REACTOME pathways (Croft et al., 2011) and KEGG pathways (Kanehisa and Goto, 2000). All the plots were generated with in-house R scripts using the packages ggplot2 and ComplexHeatmap (Gu et al., 2016; Wickham, 2016). The expression levels of DCP1a and DCP1b for different cancer types in TCGA were download from PanCanAtlas (Cancer Genome Atlas Research et al., 2013).

RESULTS

Knockout of human DCP1 represses the general mRNA decapping process *in vivo*

To investigate the roles of the two DCP1 paralogs, we knocked out DCP1a, DCP1b, or both in HEK-293T cells using the CRISPR-Cas9 technique. Western blot analysis and Sanger sequencing confirmed the successful generation of the knockout cell lines (Supplementary Figure S1). We further investigated whether the absence of DCP1a, DCP1b, or both affected decapping. To monitor mRNA decay, the NMD factor SMG7 was tethered to an mRNA reporter in the DCP1a/b-knockout cells. While DCP1 is the main decapping activator in yeast, previous studies in metazoans have shown that at least two decapping activators have to be simultaneously depleted to effectively inhibit mRNA decapping (Braun *et al.*, 2012; Sakuno et al., 2004). Surprisingly, we observed that the depletion of both DCP1a and DCP1b substantially inhibited SMG7-mediated mRNA degradation, resulting in the accumulation of deadenylated reporter RNA molecules (Figure 1A, lane 2 and 6).

To investigate whether the inhibitory effect of DCP1 knockout on decapping is specific to SMG7 or a general effect, we performed tethering assays using either the mRNA decay factor Nanos1 or the crucial miRNA component TNRC6A to induce 5′-3′ mRNA decay. In both cases, DCP1 knockout led to the substantial accumulation of mRNA decay intermediates (Supplementary Figure S2A-C), indicating that DCP1 is important for the decapping and degradation of mRNA in general.

To confirm the presence of a cap structure on the accumulated reporter RNA intermediate, we treated it with Terminator 5'-phosphate exonuclease. The resistance of the transcripts to this

treatment is strong evidence that the accumulated RNA fragments had intact 5’ caps (Figure. S2D). The accumulation of capped mRNA decay intermediates suggests slowed or impaired DCP2 mediated decapping in the absence of DCP1. Taken together, these findings provide compelling evidence for the important role of DCP1 in the decapping process in human cells, mirroring its established role in yeast.

To better understand the functional roles of the DCP1 paralogs in decapping, we performed tethering assays and reintroduced GFP-tagged DCP1a or DCP1b into DCP1a/b-knockout cells, leading in both cases to the restoration of decapping and degradation of the reporter mRNA (Figure 1B). This finding strongly suggests that DCP1a and DCP1b are functionally redundant for the general decapping of mRNA.

DCP1 EVH1 domain is crucial for cellular mRNA decapping process

Building on our finding that DCP1 is crucial for efficient mRNA decapping in human cells, we sought to identify the specific region of DCP1 that is important for the function of the decapping complex. Given the observed functional redundancy of DCP1a and DCP1b in the decapping process, we chose to use DCP1a as a model (Figure 1E). In DCP1a/b knockout cells, we overexpressed DCP1a fragments lacking either of three major domains (EVH1, HLM, TD) and monitored mRNA degradation status (Figure 1F-H). Strikingly, we observed that overexpression of a DCP1a fragment lacking EVH1 domain (ΔEVH1) could not rescue the decapping defect, indicating that this domain is crucial to coordinate the cellular decapping process. Overexpression of DCP1a without the HLM domain (ΔHLM) partially restored the decapping defect, indicating a cooperative role for this domain in coordinating DCP1's decapping function. Adequate mRNA degradation occurred in cells overexpressing DCP1a fragment without TD domain. To identify the minimal functional region of DCP1 more precisely, we generated a series of DCP1a expression constructs sequentially removing its domains. Overexpression and subsequent complementation assays in DCP1a/b-knockout cells revealed that all the constructs containing the EVH1 domain successfully restored the decapping ability of the enzyme complex (Figure 1I-K). Together, these findings indicate that the EVH1 domain is of DCP1 is essential for the formation of a functional decapping complex.

DCP1 knockout does not affect the formation of P-bodies or the enzymatic activity of DCP2

Since we observed that DCP1 appears to be indispensable for mRNA decapping, we sought to identify the precise role of DCP1 in decapping. To begin with, we explored P-body formation and DCP2 localization in DCP1a/b-knockout cells. Immunofluorescence and confocal microscopy analysis of P-body formation indicated that DCP1 has little involvement in P-body formation. In DCP1a/b-knockout cells, DCP2 remained localized in P-body granules, indicating no correlation between DCP1 and P-body formation or DCP2 localization (Figure 2A; Supplementary Figure S3).

Next, we wanted to clarify if the absence of cellular DCP1 has a direct effect on decapping activity of DCP2. To evaluate the effects of DCP1 on the decapping activity of DCP2, we performed *in vitro* decapping assays by immunoprecipitating DCP2 extracted from wild-type and DCP1a/b-knockout cells. We observed comparable enzymatic activity of DCP2 immunopurified from DCP1a/b knockout cells and WT cells, confirming that absence of cellular DCP1 do not significantly alter the inherent catalytic activity of DCP2 (Figure 2B-D). These data suggest that, in accordance with prior literature, DCP2 is sufficient for *in vitro* decapping without DCP1. (Lykke-Andersen, 2002; van Dijk *et al.*, 2002; Wang *et al.*, 2002). Nevertheless, our previous observations have emphasized the crucial role of DCP1a/b gene knockout in the *in vivo* regulation of mRNA decapping. This significance persists despite the fact that DCP2's direct decapping activity remains unaltered *in vitro*. These findings underscore the indispensable contribution of DCP1 within the complex context of authentic mRNA decapping scenarios, where multiple factors and complexities come into play.

DCP1 is a central scaffold protein that recruits multiple decapping factors to DCP2

Since the *in vitro* decapping assays did not demonstrate a significant influence of DCP1 on DCP2-mediated decapping activity, this observation could be attributed to the inherent constraints of *in vitro* assays, which often fall short of faithfully replicating the complexity of the cellular environment where multiple factors and cofactors are at play. To determine the underlying cause, we postulated that the observed cellular decapping defect in DCP1a/b knockout cells might be attributed to DCP1 functioning as a scaffold. It is conceivable that DCP1 facilitates the assembly of decapping modules, enabling their interaction with DCP2.

Alternatively, this discrepancy could stem from the unique contributions of individual subunits, such as EDC4, EDC3, DDX6, and other decapping factors, to DCP2's activity. To explore this possibility, our investigation aimed to identify the specific decapping factors that rely on DCP1 for interaction with DCP2. We overexpressed V5-SBP- or GFP-tagged DCP2 in wild-type and DCP1a/b-knockout cells and then performed coimmunoprecipitation assays with RNase A treatment. In the absence of DCP1, interactions between DCP2 and the decapping factors EDC3, DDX6, and PatL1 (Edc3, Dhh1, and Pat1 in yeast, respectively) were almost completely suppressed, but not with EDC4 (also known as Ge-1 in Drosophila), a major component of the core decapping complex in metazoans (Figure 2E). Furthermore, the interaction between DCP2 and PNRC1, as well as PNRC2, which acts in synergy with DCP1 to promote decapping, was reduced in DCP1a/b-knockout cells (Figure 2F, G). These findings suggest that DCP1 acts as a binding platform for multiple decapping factors and is essential for the interaction of these cofactors with DCP2 in human cells.

DCP2-mediated decapping is not merely due to the presence of decapping factors on the DCP1a scaffold

Based on our observation that DCP1a EVH1 domain is sufficient to rescue the decapping defect in DCP1a/b knockout cells, we hypothesized that the DCP1 EVH1 domain may play a key role in regulating the decapping machinery. To evaluate the contribution of this domain to the formation of the decapping complex, we sought to identify which decapping factors interact with the DCP1 EVH1 domain. We overexpressed full-length or fragmented GFP-tagged DCP1a in DCP1a/b-knockout cells and subsequently immunoprecipitated the protein in the presence of RNase A. The EVH1 domain of DCP1a did not interact with any of the decapping factors except for DCP2 and PNRC1/2 (Figure. 3A-D).

PNRC1 has been shown to interact with the NMD factor UPF1, indicating that it is involved in the NMD pathway (Cho *et al.*, 2009). Furthermore, it has recently been shown that PNRC1 serves as a regulator of rRNA maturation within nucleoli, tightly controlling the process of ribosomal RNA maturation (Gaviraghi *et al.*, 2018). Previous studies have also demonstrated the involvement of PNRC2 in the NMD pathway. Structural analysis of the PNRC2-DCP1a complex has shown that PNRC2 can directly activate the decapping process (Cho et al., 2013; Cho *et al.*,

2009; Lai et al., 2012). Given this background, we investigated the functional role of PNRC1/2 in modulating the activity of DCP2 through DCP1 EVH1 domain.

To determine whether PNRC1 and PNRC2 are necessary for DCP2 activity *in vivo*, we used shRNA to knockdown the expression of PNRC1 and PNRC2 individually (Supplemental Figure S4). Unlike the DCP1 knockout, the knockdown of PNRC1 or PNRC2 had only a minor effect on the results of the tethering assays, suggesting that PNRC1 and PNRC2 are not essential for DCP2 activity (Figure 3E, F). Therefore, we concluded the activation of the decapping complex by the DCP1a cannot be solely attributed to the binding of decapping factors on the DCP1a scaffold.

DCP1 increases the mRNA-binding affinity of DCP2

Our findings suggest that the marked reduction in decapping activity observed in DCP1a/b-knockout cells is not exclusively essential for DCP1's function as a scaffold in the decapping process. This discrepancy prompts an investigation into the potential role of the DCP1 EVH1 domain, as previous studies have theorized its critical involvement in DCP2 mRNA binding (Chang *et al.*, 2014; Valkov *et al.*, 2016), although this aspect has not been explored to date. To evaluate this hypothesis, we investigated the molecular mechanisms of DCP1-mediated substrate binding by DCP2.

We evaluated the impact of DCP1 on interactions between DCP2 and mRNA in human cells using tethering assays with a catalytically inactive mutant DCP2 protein (DCP2 E148Q) introduced into DCP1a/b-knockout cells. This prevented the degradation of target mRNAs and maintained them in the decapping stage. Full-length DCP1a or the EVH1 domain alone were also introduced into the cells (Figure 3G). DCP2 samples were then immunoprecipitated and real-time PCR was used to measure the concentrations of reporter mRNAs that interacted with DCP2. Our results show that the mRNA binding affinity of DCP2 is weak in the absence of DCP1 but significantly increases in the presence of DCP1a full-length or the EVH1 domain (Figure 3H, I).

To further bolster the validity of these findings, we conducted RNA immunoprecipitation (RNA-IP) assays. Reporter RNA was isolated during the decapping process and consistent with the findings of the DCP2 immunoprecipitation assays, high levels of DCP2 were observed in the

RNA immunoprecipitation assays when the DCP1a EVH1 domain was overexpressed (Figure 3J). These findings strongly underscore the significance of the EVH1 domain of DCP1a in enhancing interactions between DCP2 and mRNA.

Taken together, we demonstrated that DCP1a can regulate DCP2's cellular decapping activity by enhancing DCP2's affinty to RNA, in addition to bridging the interactions of DCP2 with other decapping factors. This represents a pivotal molecular mechanism by which DCP1a exerts its regulatory control over the mRNA decapping process.

DCP1a and DCP1b regulate distinct endogenous mRNA targets

The existence of two apparently redundant DCP1 paralogs, DCP1a and DCP1b, is intriguing, and raises the question whether they are truly redundant or in fact have distinct roles. Considering the low sequence similarity of DCP1a and DCP1b and since DCP1 was observed to enhance mRNA recognition by DCP2, we hypothesized that the DCP1 paralogs may contribute to the preferential regulation of specific mRNA targets. In other words, although DCP1a and DCP1b may be redundant in the general mRNA decapping process, they may differentially regulate specific mRNA targets.

We performed an RNA-Seq analysis of HEK-293T cells lacking DCP1a, DCP1b, or both and compared the results with those from wild-type cells (Figure 4A; Supplementary Figure S5A-D). There were significant differences in the transcript profiles of the knockout cells. In DCP1a-, DCP1b-, and DCP1a/b-knockout cells, the expression of 604, 1,255, and 1,146 genes was significantly upregulated, while 504, 677, and 1,383 genes were significantly downregulated. Notably, only a subset of genes dysregulated in both DCP1a- and DCP1b-knockout cells showed alterations in DCP1a/b-knockout cells. This suggests that the disruption of the decapping process in DCP1a/b-knockout cells results in the accumulation of unprocessed mRNA intermediates. This observation is further evidence of the crucial role of DCP1 in decapping (Figure 4B). Furthermore, the transcriptomes of the DCP1a- and DCP1b-knockout cells differed from the transcriptome of wild-type cells, indicating that these two proteins control distinct sets of genes, and therefore that DCP1a and DCP1b have non-redundant roles in the regulation of gene expression.

DCP1a and DCP1b play distinct roles in cancer and gene expression regulation

To identify the gene sets associated with DCP1a and DCP1b, we performed GSEA for Hallmark, Gene Ontology (GO), Kyoto Encyclopedia of Genes and Genomes (KEGG), and REACTOM pathways using the transcriptome data from DCP1a and DCP1b knockout experiments. Analysis of the Hallmark pathways revealed that multiple cancer-related pathways were activated in DCP1a-knockout and/or DCP1b-knockout cells, such as apoptosis, E2F targets, MYC targets, the mTOR signalling pathway, the G2/M checkpoint pathway, the KRAS signalling pathway, and the epithelial–mesenchymal transition pathway (Figure 4C). Results for the GO, KEGG and REACTOM pathways likewise showed that DCP1a is involved in other cancer-related pathways, such as the Notch signalling pathway, embryonic skeletal system development, vasculature development, and the mitotic cell cycle pathway (Figure 4D; Supplementary Figure S5E–H). These results are consistent with recent findings that DCP1a is strongly associated with embryonic growth and tumour development (Ibayashi et al., 2021; Wu et al., 2018; Wu et al., 2021a), and suggest that DCP1a is more strongly associated with cancer than is DCP1b. Furthermore, we noted that the activation of capped intron-containing pre-mRNA processing was evident in both DCP1a- and DCP1b-deficient cells (Supplementary Figure S5H). This observation aligns with the understanding that the depletion of DCP1a not only diminishes mRNA degradation and transcription but also underscores the pivotal role of DCP1 in the orchestration of gene expression. To further assess the clinical relevance of our findings, we evaluated the expression levels of DCP1a and DCP1b using data from The Cancer Genome Atlas (TCGA) database (Figure 4E). Consistent with the above results, we found that expression levels of DCP1a were reduced in various cancers: bladder urothelial carcinoma, uterine corpus endometrial carcinoma, head and neck squamous cell carcinoma, prostate adenocarcinoma, cervical squamous cell carcinoma and endocervical adenocarcinoma, lung squamous cell carcinoma, kidney renal clear cell carcinoma, breast invasive carcinoma, thyroid carcinoma, lung adenocarcinoma, pheochromocytoma and paraganglioma, and thymoma. In contrast, DCP1b exhibited significant upregulation in certain cancer types while showing downregulation in others. This suggests that the role of DCP1b in tumorigenesis is multifaceted and context-dependent. In summary, these findings indicate that DCP1a and DCP1b likely have distinct and non-redundant roles in the development and progression of cancer. The nuanced functions of

DCP1a and DCP1b in the context of tumorigenesis warrant further investigation to fully elucidate their specific contributions to cancer pathogenesis. Hence, in future research, a comparative analysis should be conducted to gain a deeper understanding of their involvement in cancer, specifically concerning the interconnection between DCP1a/b and cancer in order to comprehensively explore the relevance of DCP1 in human physiology.

DCP1a and DCP1b play different roles in cellular metabolism

To comprehensively explore the effects of DCP1a and DCP1b knockout, we further conducted untargeted metabolomic profiling of DCP1a-, DCP1b-, and DCP1a/b-knockout cells. This analysis sheds light on the distinct roles of these proteins. After removing features that appeared in control samples and manually removing features with a poor peak shape and extremely low abundance, we identified approximately 123 metabolites in the experimental samples. We successfully differentiated DCP1a- and DCP1b-knockout cells using PLS-DA score plots, loading plots, and heatmaps of the metabolomic data and the differences in the metabolomic profiles revealed the distinct impacts of DCP1a and DCP1b on cellular metabolism (Figure 5A; Supplementary Figure S6A, B). Additionally, the volcano plots illustrated the significant metabolic disparities among DCP1a-, DCP1b-, and DCP1a/b-knockout cells (Figure 5B-D), emphasizing the presence of noticeable differences. Remarkably, uridine diphosphate (UDP)-N-acetylglucosamine (GlcNAc), GlcNAc, glycerophosphoserine, and glycerophosphocholine levels were significantly elevated in DCP1a- and DCP1a/b-knockout cells, whereas those of nicotinamide adenine dinucleotide (NAD) were reduced. By contrast, DCP1b-knockout cells had elevated levels of lysophosphatidylethanolamine (P-18:0) [LPE (P-18:0)] (Figure 5E, F; Supplementary Figure S6C). These results suggest that DCP1a and DCP1b have different effects on these metabolic pathways.

The significantly altered metabolites in the DCP1-knockout cells included UDP–GlcNAc and GlcNAc, which are associated with the amino sugar and nucleotide sugar metabolism pathway (hsa00520) in KEGG (Supplementary Figure S7). Further investigation revealed that the levels of these metabolites are correlated with the transcript levels associated with the amino sugar and nucleotide sugar metabolism pathway (Figure 5G). Together, our data strongly imply that DCP1a and DCP1b may exert regulatory influence over UDP-GlcNAc and GlcNAc through

pathways that extend beyond the scope of amino sugar and nucleotide sugar metabolism. This indicates that these proteins play intricate and far-reaching roles in modulating cellular metabolism. Further studies are necessary to unravel the specific mechanisms and pathways by which DCP1a and DCP1b control these metabolites and to fully elucidate their roles in cellular metabolism.

DISCUSSION

In this study, we found that DCP1 plays a key role in promoting mRNA decapping in human cells. The double knockout of DCP1a and DCP1b resulted in a significant increase in the stability of the tethered mRNA reporter. We also verified that DCP1 is not only a key platform for assembling various mRNA decapping cofactors, but also established that the EVH1 domain of DCP1 is critical for the mRNA decapping process. Through RNA immunoprecipitation assays, we discovered that the interactions between DCP2 and mRNA heavily rely on the presence of DCP1's EVH1 domain. These findings imply that DCP1 facilitates the binding of DCP2 to target mRNAs through multiple mechanisms, thereby enhancing the efficiency of mRNA decapping. Finally, our integrated transcriptome and metabolome analyses comparing the specific functions of DCP1a and DCP1b in human cells revealed that they can regulate distinct endogenous mRNA targets and biological processes.

In a prior investigation, we made an intriguing discovery. In human cells, substituting the conserved NR-loop with a flexible GSSG loop in the EVH1 domain of DCP1 had no adverse effect on the interaction between DCP1 and DCP2, nor did it impede their integration into decapping factors. However, this seemingly subtle alteration had a significant consequence – it disrupted the activation of DCP2 (Chang *et al.*, 2014). This points to the pivotal role played by the EVH1 domain of DCP1 in the activation of DCP2, which, in turn, is a critical step in the mRNA decapping process. These findings, combined with our findings in the present study, provide compelling evidence that the DCP1 EVH1 domain is not just a passive component but a crucial player in coordinating interactions and facilitating conformational changes necessary for efficient mRNA decapping. A comprehensive functional characterization of these mechanisms is imperative to fully elucidate the mechanisms underlying DCP1-mediated activation of decapping.

While the protein components of the mRNA decapping machinery have been identified, our current understanding of the distinct roles played by individual decapping factors throughout the process remains limited. Notably, whether the different decapping factors confer target specificity has yet to be clarified. Although previous studies have suggested that DCP1a and DCP1b, the two paralogs of DCP1, play redundant roles in general mRNA decay, this notion is mainly based on reporter assays and single-gene approaches. The specific regulation of endogenous mRNA targets and biological processes by DCP1a and DCP1b is yet to be elucidated.

In this study, we investigated potential functional differences between DCP1a and DCP1b through a combined transcriptome and metabolome analysis. While DCP1a and DCP1b have both been implicated in cancer, our observation of significant alterations in multiple cancer-related pathways in DCP1a-knockout cells suggests that DCP1a is more prominently associated with cancer development. Furthermore, the downregulation of DCP1a in multiple cancer types further supports the concept that DCP1a is a cancer-associated gene and suggests that its dysregulation may play a contributory role in the onset and progression of diverse cancers. (Ibayashi *et al.*, 2021; Wu *et al.*, 2018; Wu *et al.*, 2021a). Nevertheless, it is important to note that DCP1b is also cancer-related, and further studies are required to fully understand its role in cancer pathogenesis.

Our scrutiny of the transcript profiles and metabolite levels within DCP1a- and DCP1b-knockout cells has unveiled their unique contributions to cellular processes. While DCP1a and DCP1b do exhibit certain common gene targets, their functions are not entirely interchangeable. Pathway analysis indicated that DCP1a and DCP1b may have partially complementary roles in the regulation of cellular pathways. Additionally, several metabolites showed notable alterations in knockout cells, potentially opening a new avenue for investigating the metabolic consequences of DCP1 knockout. Our findings yield valuable understanding of the distinct functions of DCP1a and DCP1b in human cells and the complex regulatory mechanisms underlying cellular metabolism. The potential targets we identified could be investigated further by quantifying specific transcripts and metabolites, and a larger sample size would facilitate the identification of correlations between differentially expressed genes and differentially abundant metabolites.

Overall, our study provides valuable insights into the molecular mechanisms governing DCP1-mediated decapping in human cells and the coordinated regulation of DCP1a and DCP1b, which has important implications for gene expression and cellular function. Future biochemical characterization of the specific mRNA targets and biological pathways regulated by DCP1a and DCP1b is necessary to fully elucidate their roles. This information may help uncover the precise mechanisms underlying mRNA decapping and gene regulation. Furthermore, studying the dysregulation of DCP1 paralogs, especially in cancer, may reveal potential therapeutic targets and improve treatment strategies.

DATA AVAILABILITY

Raw sequencing reads and processed data files containing the read counts and normalized abundance measurements generated in this study were deposited in the GEO under the accession number of GSE230847.

SUPPLEMENTARY DATA

Supplementary Data are available at *eLife* online.

ACKNOWLEDGMENT

We dedicate this work to Elisa Izaurralde who passed away during the study period. We thank Sigrun Helms and Heike Budde for their technical assistance. We thank the Metabolomics Core Laboratory, Centers of Genomic and Precision Medicine, National Taiwan University for the instrumental support.

FUNDING

This work was supported by the Max Planck Society, the Higher Education Sprout Project by the Ministry of Education (MOE) in Taiwan, National Science and Technology Council, Taiwan [MOST109-2311-B-010-001-MY2], and Yen Tjing Ling Medical Foundation [CI-110-17].

CONFLICT OF INTEREST

None declared

REFERENCES

Ahmed, I., Buchert, R., Zhou, M., Jiao, X., Mittal, K., Sheikh, T.I., Scheller, U., Vasli, N., Rafiq, M.A., Brohi, M.Q., et al. (2015). Mutations in DCPS and EDC3 in autosomal recessive intellectual disability indicate a crucial role for mRNA decapping in neurodevelopment. Hum Mol Genet *24*, 3172-3180. 10.1093/hmg/ddv069.

Arribas-Layton, M., Wu, D., Lykke-Andersen, J., and Song, H. (2013). Structural and functional control of the eukaryotic mRNA decapping machinery. Biochim Biophys Acta *1829*, 580-589. 10.1016/j.bbagrm.2012.12.006.

Beelman, C.A., Stevens, A., Caponigro, G., LaGrandeur, T.E., Hatfield, L., Fortner, D.M., and Parker, R. (1996). An essential component of the decapping enzyme required for normal rates of mRNA turnover. Nature *382*, 642-646. 10.1038/382642a0.

Bolger, A.M., Lohse, M., and Usadel, B. (2014). Trimmomatic: a flexible trimmer for Illumina sequence data. Bioinformatics *30*, 2114-2120. 10.1093/bioinformatics/btu170.

Braun, J.E., Truffault, V., Boland, A., Huntzinger, E., Chang, C.T., Haas, G., Weichenrieder, O., Coles, M., and Izaurralde, E. (2012). A direct interaction between DCP1 and XRN1 couples mRNA decapping to 5' exonucleolytic degradation. Nat Struct Mol Biol *19*, 1324-1331. 10.1038/nsmb.2413.

Calviello, L., Mukherjee, N., Wyler, E., Zauber, H., Hirsekorn, A., Selbach, M., Landthaler, M., Obermayer, B., and Ohler, U. (2016). Detecting actively translated open reading frames in ribosome profiling data. Nat Methods *13*, 165-170. 10.1038/nmeth.3688.

Cancer Genome Atlas Research, N., Weinstein, J.N., Collisson, E.A., Mills, G.B., Shaw, K.R., Ozenberger, B.A., Ellrott, K., Shmulevich, I., Sander, C., and Stuart, J.M. (2013). The Cancer Genome Atlas Pan-Cancer analysis project. Nat Genet *45*, 1113-1120. 10.1038/ng.2764.

Chang, C.T., Bercovich, N., Loh, B., Jonas, S., and Izaurralde, E. (2014). The activation of the decapping enzyme DCP2 by DCP1 occurs on the EDC4 scaffold and involves a conserved loop in DCP1. Nucleic Acids Res *42*, 5217-5233. 10.1093/nar/gku129.

Chang, C.T., Muthukumar, S., Weber, R., Levdansky, Y., Chen, Y., Bhandari, D., Igreja, C., Wohlbold, L., Valkov, E., and Izaurralde, E. (2019). A low-complexity region in human XRN1 directly recruits deadenylation and decapping factors in 5'-3' messenger RNA decay. Nucleic Acids Res *47*, 9282-9295. 10.1093/nar/gkz633.

Charenton, C., Gaudon-Plesse, C., Back, R., Ulryck, N., Cosson, L., Seraphin, B., and Graille, M. (2020). Pby1 is a direct partner of the Dcp2 decapping enzyme. Nucleic Acids Res *48*, 6353-6366. 10.1093/nar/gkaa337.

Charenton, C., Gaudon-Plesse, C., Fourati, Z., Taverniti, V., Back, R., Kolesnikova, O., Seraphin, B., and Graille, M. (2017). A unique surface on Pat1 C-terminal domain directly interacts with Dcp2 decapping enzyme and Xrn1 5'-3' mRNA exonuclease in yeast. Proc Natl Acad Sci U S A *114*, E9493-E9501. 10.1073/pnas.1711680114.

Charenton, C., and Graille, M. (2018). mRNA decapping: finding the right structures. Philos Trans R Soc Lond B Biol Sci *373*. 10.1098/rstb.2018.0164.

Charenton, C., Taverniti, V., Gaudon-Plesse, C., Back, R., Seraphin, B., and Graille, M. (2016). Structure of the active form of Dcp1-Dcp2 decapping enzyme bound to m(7)GDP and its Edc3 activator. Nat Struct Mol Biol *23*, 982-986. 10.1038/nsmb.3300.

Chen, C.A., and Shyu, A.B. (2017). Emerging Themes in Regulation of Global mRNA Turnover in cis. Trends Biochem Sci *42*, 16-27. 10.1016/j.tibs.2016.08.014.

Chen, C.Y., and Shyu, A.B. (2003). Rapid deadenylation triggered by a nonsense codon precedes decay of the RNA body in a mammalian cytoplasmic nonsense-mediated decay pathway. Mol Cell Biol *23*, 4805-4813. 10.1128/MCB.23.14.4805-4813.2003.

Chen, C.Y., and Shyu, A.B. (2011). Mechanisms of deadenylation-dependent decay. Wiley Interdiscip Rev RNA *2*, 167-183. 10.1002/wrna.40.

Cho, H., Han, S., Choe, J., Park, S.G., Choi, S.S., and Kim, Y.K. (2013). SMG5-PNRC2 is functionally dominant compared with SMG5-SMG7 in mammalian nonsense-mediated mRNA decay. Nucleic Acids Res *41*, 1319-1328. 10.1093/nar/gks1222.
Cho, H., Kim, K.M., and Kim, Y.K. (2009). Human proline-rich nuclear receptor coregulatory protein 2 mediates an interaction between mRNA surveillance machinery and decapping complex. Mol Cell *33*, 75-86. 10.1016/j.molcel.2008.11.022.
Corbett, A.H. (2018). Post-transcriptional regulation of gene expression and human disease. Curr Opin Cell Biol *52*, 96-104. 10.1016/j.ceb.2018.02.011.
Croft, D., O'Kelly, G., Wu, G., Haw, R., Gillespie, M., Matthews, L., Caudy, M., Garapati, P., Gopinath, G., Jassal, B., et al. (2011). Reactome: a database of reactions, pathways and biological processes. Nucleic Acids Res *39*, D691-697. 10.1093/nar/gkq1018.
Decker, C.J., and Parker, R. (1993). A turnover pathway for both stable and unstable mRNAs in yeast: evidence for a requirement for deadenylation. Genes Dev *7*, 1632-1643. 10.1101/gad.7.8.1632.
Deshmukh, M.V., Jones, B.N., Quang-Dang, D.U., Flinders, J., Floor, S.N., Kim, C., Jemielity, J., Kalek, M., Darzynkiewicz, E., and Gross, J.D. (2008). mRNA decapping is promoted by an RNA-binding channel in Dcp2. Mol Cell *29*, 324-336. 10.1016/j.molcel.2007.11.027.
Dunckley, T., and Parker, R. (1999). The DCP2 protein is required for mRNA decapping in Saccharomyces cerevisiae and contains a functional MutT motif. EMBO J *18*, 5411-5422. 10.1093/emboj/18.19.5411.
Eberle, A.B., Lykke-Andersen, S., Muhlemann, O., and Jensen, T.H. (2009). SMG6 promotes endonucleolytic cleavage of nonsense mRNA in human cells. Nat Struct Mol Biol *16*, 49-55. 10.1038/nsmb.1530.
Eulalio, A., Behm-Ansmant, I., and Izaurralde, E. (2007). P bodies: at the crossroads of post-transcriptional pathways. Nat Rev Mol Cell Biol *8*, 9-22. 10.1038/nrm2080.
Fenger-Gron, M., Fillman, C., Norrild, B., and Lykke-Andersen, J. (2005). Multiple processing body factors and the ARE binding protein TTP activate mRNA decapping. Mol Cell *20*, 905-915. 10.1016/j.molcel.2005.10.031.
Floor, S.N., Jones, B.N., Hernandez, G.A., and Gross, J.D. (2010). A split active site couples cap recognition by Dcp2 to activation. Nat Struct Mol Biol *17*, 1096-1101. 10.1038/nsmb.1879.
Fourati, Z., Kolesnikova, O., Back, R., Keller, J., Charenton, C., Taverniti, V., Plesse, C.G., Lazar, N., Durand, D., van Tilbeurgh, H., et al. (2014). The C-terminal domain from S. cerevisiae Pat1 displays two conserved regions involved in decapping factor recruitment. PLoS One *9*, e96828. 10.1371/journal.pone.0096828.
Frankish, A., Diekhans, M., Ferreira, A.M., Johnson, R., Jungreis, I., Loveland, J., Mudge, J.M., Sisu, C., Wright, J., Armstrong, J., et al. (2019). GENCODE reference annotation for the human and mouse genomes. Nucleic Acids Res *47*, D766-D773. 10.1093/nar/gky955.
Fromm, S.A., Truffault, V., Kamenz, J., Braun, J.E., Hoffmann, N.A., Izaurralde, E., and Sprangers, R. (2012). The structural basis of Edc3- and Scd6-mediated activation of the Dcp1:Dcp2 mRNA decapping complex. EMBO J *31*, 279-290. 10.1038/emboj.2011.408.
Fukuhara, N., Ebert, J., Unterholzner, L., Lindner, D., Izaurralde, E., and Conti, E. (2005). SMG7 is a 14-3-3-like adaptor in the nonsense-mediated mRNA decay pathway. Mol Cell *17*, 537-547. 10.1016/j.molcel.2005.01.010.
Furuichi, Y., LaFiandra, A., and Shatkin, A.J. (1977). 5'-Terminal structure and mRNA stability. Nature *266*, 235-239. 10.1038/266235a0.
Garneau, N.L., Wilusz, J., and Wilusz, C.J. (2007). The highways and byways of mRNA decay. Nat Rev Mol Cell Biol *8*, 113-126. 10.1038/nrm2104.
Gaviraghi, M., Vivori, C., Pareja Sanchez, Y., Invernizzi, F., Cattaneo, A., Santoliquido, B.M., Frenquelli, M., Segalla, S., Bachi, A., Doglioni, C., et al. (2018). Tumor suppressor PNRC1 blocks rRNA maturation by recruiting the decapping complex to the nucleolus. EMBO J *37*. 10.15252/embj.201899179.

Gu, Z., Eils, R., and Schlesner, M. (2016). Complex heatmaps reveal patterns and correlations in multidimensional genomic data. Bioinformatics *32*, 2847-2849. 10.1093/bioinformatics/btw313.
Guijas, C., Montenegro-Burke, J.R., Domingo-Almenara, X., Palermo, A., Warth, B., Hermann, G., Koellensperger, G., Huan, T., Uritboonthai, W., Aisporna, A.E., et al. (2018). METLIN: A Technology Platform for Identifying Knowns and Unknowns. Anal Chem *90*, 3156-3164. 10.1021/acs.analchem.7b04424.
He, F., and Jacobson, A. (2015). Control of mRNA decapping by positive and negative regulatory elements in the Dcp2 C-terminal domain. RNA *21*, 1633-1647. 10.1261/rna.052449.115.
He, F., and Jacobson, A. (2022). Eukaryotic mRNA decapping factors: molecular mechanisms and activity. FEBS J. 10.1111/febs.16626.
He, F., Wu, C., and Jacobson, A. (2022). Dcp2 C-terminal cis-binding elements control selective targeting of the decapping enzyme by forming distinct decapping complexes. Elife *11*. 10.7554/eLife.74410.
Hsu, C.L., and Stevens, A. (1993). Yeast cells lacking 5'-->3' exoribonuclease 1 contain mRNA species that are poly(A) deficient and partially lack the 5' cap structure. Mol Cell Biol *13*, 4826-4835. 10.1128/mcb.13.8.4826-4835.1993.
Huntzinger, E., Kashima, I., Fauser, M., Sauliere, J., and Izaurralde, E. (2008). SMG6 is the catalytic endonuclease that cleaves mRNAs containing nonsense codons in metazoan. RNA *14*, 2609-2617. 10.1261/rna.1386208.
Ibayashi, M., Aizawa, R., and Tsukamoto, S. (2021). mRNA decapping factor Dcp1a is essential for embryonic growth in mice. Biochem Biophys Res Commun *555*, 128-133. 10.1016/j.bbrc.2021.03.117.
Jakymiw, A., Lian, S., Eystathioy, T., Li, S., Satoh, M., Hamel, J.C., Fritzler, M.J., and Chan, E.K. (2005). Disruption of GW bodies impairs mammalian RNA interference. Nat Cell Biol *7*, 1267-1274. 10.1038/ncb1334.
Jonas, S., and Izaurralde, E. (2013). The role of disordered protein regions in the assembly of decapping complexes and RNP granules. Genes Dev *27*, 2628-2641. 10.1101/gad.227843.113.
Jonas, S., and Izaurralde, E. (2015). Towards a molecular understanding of microRNA-mediated gene silencing. Nat Rev Genet *16*, 421-433. 10.1038/nrg3965.
Kanehisa, M., and Goto, S. (2000). KEGG: kyoto encyclopedia of genes and genomes. Nucleic Acids Res *28*, 27-30. 10.1093/nar/28.1.27.
Lai, T., Cho, H., Liu, Z., Bowler, M.W., Piao, S., Parker, R., Kim, Y.K., and Song, H. (2012). Structural basis of the PNRC2-mediated link between mrna surveillance and decapping. Structure *20*, 2025-2037. 10.1016/j.str.2012.09.009.
Li, B., and Dewey, C.N. (2011). RSEM: accurate transcript quantification from RNA-Seq data with or without a reference genome. BMC Bioinformatics *12*, 323. 10.1186/1471-2105-12-323.
Lim, J., Lee, M., Son, A., Chang, H., and Kim, V.N. (2016). mTAIL-seq reveals dynamic poly(A) tail regulation in oocyte-to-embryo development. Genes Dev *30*, 1671-1682. 10.1101/gad.284802.116.
Ling, S.H., Qamra, R., and Song, H. (2011). Structural and functional insights into eukaryotic mRNA decapping. Wiley Interdiscip Rev RNA *2*, 193-208. 10.1002/wrna.44.
Lobel, J.H., and Gross, J.D. (2020). Pdc2/Pat1 increases the range of decay factors and RNA bound by the Lsm1-7 complex. RNA *26*, 1380-1388. 10.1261/rna.075812.120.
Lobel, J.H., Tibble, R.W., and Gross, J.D. (2019). Pat1 activates late steps in mRNA decay by multiple mechanisms. Proc Natl Acad Sci U S A *116*, 23512-23517. 10.1073/pnas.1905455116.
Loh, B., Jonas, S., and Izaurralde, E. (2013). The SMG5-SMG7 heterodimer directly recruits the CCR4-NOT deadenylase complex to mRNAs containing nonsense codons via interaction with POP2. Genes Dev *27*, 2125-2138. 10.1101/gad.226951.113.
Love, M.I., Huber, W., and Anders, S. (2014). Moderated estimation of fold change and dispersion for RNA-seq data with DESeq2. Genome Biol *15*, 550. 10.1186/s13059-014-0550-8.
Luo, Y., Na, Z., and Slavoff, S.A. (2018). P-Bodies: Composition, Properties, and Functions. Biochemistry *57*, 2424-2431. 10.1021/acs.biochem.7b01162.

Lykke-Andersen, J. (2002). Identification of a human decapping complex associated with hUpf proteins in nonsense-mediated decay. Mol Cell Biol *22*, 8114-8121. 10.1128/MCB.22.23.8114-8121.2002.
Lykke-Andersen, J., Shu, M.D., and Steitz, J.A. (2000). Human Upf proteins target an mRNA for nonsense-mediated decay when bound downstream of a termination codon. Cell *103*, 1121-1131. 10.1016/s0092-8674(00)00214-2.
Metze, S., Herzog, V.A., Ruepp, M.D., and Muhlemann, O. (2013). Comparison of EJC-enhanced and EJC-independent NMD in human cells reveals two partially redundant degradation pathways. RNA *19*, 1432-1448. 10.1261/rna.038893.113.
Mugridge, J.S., Coller, J., and Gross, J.D. (2018a). Structural and molecular mechanisms for the control of eukaryotic 5'-3' mRNA decay. Nat Struct Mol Biol *25*, 1077-1085. 10.1038/s41594-018-0164-z.
Mugridge, J.S., Tibble, R.W., Ziemniak, M., Jemielity, J., and Gross, J.D. (2018b). Structure of the activated Edc1-Dcp1-Dcp2-Edc3 mRNA decapping complex with substrate analog poised for catalysis. Nat Commun *9*, 1152. 10.1038/s41467-018-03536-x.
Mugridge, J.S., Ziemniak, M., Jemielity, J., and Gross, J.D. (2016). Structural basis of mRNA-cap recognition by Dcp1-Dcp2. Nat Struct Mol Biol *23*, 987-994. 10.1038/nsmb.3301.
Ng, C.K., Shboul, M., Taverniti, V., Bonnard, C., Lee, H., Eskin, A., Nelson, S.F., Al-Raqad, M., Altawalbeh, S., Seraphin, B., and Reversade, B. (2015). Loss of the scavenger mRNA decapping enzyme DCPS causes syndromic intellectual disability with neuromuscular defects. Hum Mol Genet *24*, 3163-3171. 10.1093/hmg/ddv067.
Piccirillo, C., Khanna, R., and Kiledjian, M. (2003). Functional characterization of the mammalian mRNA decapping enzyme hDcp2. RNA *9*, 1138-1147. 10.1261/rna.5690503.
Rohart, F., Gautier, B., Singh, A., and Le Cao, K.A. (2017). mixOmics: An R package for 'omics feature selection and multiple data integration. PLoS Comput Biol *13*, e1005752. 10.1371/journal.pcbi.1005752.
Sakuno, T., Araki, Y., Ohya, Y., Kofuji, S., Takahashi, S., Hoshino, S., and Katada, T. (2004). Decapping reaction of mRNA requires Dcp1 in fission yeast: its characterization in different species from yeast to human. J Biochem *136*, 805-812. 10.1093/jb/mvh190.
Sgromo, A., Raisch, T., Backhaus, C., Keskeny, C., Alva, V., Weichenrieder, O., and Izaurralde, E. (2018). Drosophila Bag-of-marbles directly interacts with the CAF40 subunit of the CCR4-NOT complex to elicit repression of mRNA targets. RNA *24*, 381-395. 10.1261/rna.064584.117.
Sharif, H., and Conti, E. (2013). Architecture of the Lsm1-7-Pat1 complex: a conserved assembly in eukaryotic mRNA turnover. Cell Rep *5*, 283-291. 10.1016/j.celrep.2013.10.004.
She, M., Decker, C.J., Chen, N., Tumati, S., Parker, R., and Song, H. (2006). Crystal structure and functional analysis of Dcp2p from Schizosaccharomyces pombe. Nat Struct Mol Biol *13*, 63-70. 10.1038/nsmb1033.
She, M., Decker, C.J., Svergun, D.I., Round, A., Chen, N., Muhlrad, D., Parker, R., and Song, H. (2008). Structural basis of dcp2 recognition and activation by dcp1. Mol Cell *29*, 337-349. 10.1016/j.molcel.2008.01.002.
Steiger, M., Carr-Schmid, A., Schwartz, D.C., Kiledjian, M., and Parker, R. (2003). Analysis of recombinant yeast decapping enzyme. RNA *9*, 231-238. 10.1261/rna.2151403.
Stevens, A. (1988). mRNA-decapping enzyme from Saccharomyces cerevisiae: purification and unique specificity for long RNA chains. Mol Cell Biol *8*, 2005-2010. 10.1128/mcb.8.5.2005-2010.1988.
Subramanian, A., Tamayo, P., Mootha, V.K., Mukherjee, S., Ebert, B.L., Gillette, M.A., Paulovich, A., Pomeroy, S.L., Golub, T.R., Lander, E.S., and Mesirov, J.P. (2005). Gene set enrichment analysis: a knowledge-based approach for interpreting genome-wide expression profiles. Proc Natl Acad Sci U S A *102*, 15545-15550. 10.1073/pnas.0506580102.
Subtelny, A.O., Eichhorn, S.W., Chen, G.R., Sive, H., and Bartel, D.P. (2014). Poly(A)-tail profiling reveals an embryonic switch in translational control. Nature *508*, 66-71. 10.1038/nature13007.
The Gene Ontology, C. (2019). The Gene Ontology Resource: 20 years and still GOing strong. Nucleic Acids Res *47*, D330-D338. 10.1093/nar/gky1055.

Tibble, R.W., Depaix, A., Kowalska, J., Jemielity, J., and Gross, J.D. (2021). Biomolecular condensates amplify mRNA decapping by biasing enzyme conformation. Nat Chem Biol *17*, 615-623. 10.1038/s41589-021-00774-x.
Topisirovic, I., Svitkin, Y.V., Sonenberg, N., and Shatkin, A.J. (2011). Cap and cap-binding proteins in the control of gene expression. Wiley Interdiscip Rev RNA *2*, 277-298. 10.1002/wrna.52.
Tritschler, F., Eulalio, A., Truffault, V., Hartmann, M.D., Helms, S., Schmidt, S., Coles, M., Izaurralde, E., and Weichenrieder, O. (2007). A divergent Sm fold in EDC3 proteins mediates DCP1 binding and P-body targeting. Mol Cell Biol *27*, 8600-8611. 10.1128/MCB.01506-07.
Valkov, E., Muthukumar, S., Chang, C.T., Jonas, S., Weichenrieder, O., and Izaurralde, E. (2016). Structure of the Dcp2-Dcp1 mRNA-decapping complex in the activated conformation. Nat Struct Mol Biol *23*, 574-579. 10.1038/nsmb.3232.
van Dijk, E., Cougot, N., Meyer, S., Babajko, S., Wahle, E., and Seraphin, B. (2002). Human Dcp2: a catalytically active mRNA decapping enzyme located in specific cytoplasmic structures. EMBO J *21*, 6915-6924. 10.1093/emboj/cdf678.
Vidya, E., and Duchaine, T.F. (2022). Eukaryotic mRNA Decapping Activation. Front Genet *13*, 832547. 10.3389/fgene.2022.832547.
Wang, Z., Jiao, X., Carr-Schmid, A., and Kiledjian, M. (2002). The hDcp2 protein is a mammalian mRNA decapping enzyme. Proc Natl Acad Sci U S A *99*, 12663-12668. 10.1073/pnas.192445599.
Webster, M.W., Chen, Y.H., Stowell, J.A.W., Alhusaini, N., Sweet, T., Graveley, B.R., Coller, J., and Passmore, L.A. (2018). mRNA Deadenylation Is Coupled to Translation Rates by the Differential Activities of Ccr4-Not Nucleases. Mol Cell *70*, 1089-1100 e1088. 10.1016/j.molcel.2018.05.033.
Wickham, H. (2016). ggplot2: Elegant Graphics for Data Analysis (Springer-Verlag New York).
Wishart, D.S., Feunang, Y.D., Marcu, A., Guo, A.C., Liang, K., Vazquez-Fresno, R., Sajed, T., Johnson, D., Li, C., Karu, N., et al. (2018). HMDB 4.0: the human metabolome database for 2018. Nucleic Acids Res *46*, D608-D617. 10.1093/nar/gkx1089.
Wu, C., Zhu, X., Tao, K., Liu, W., Ruan, T., Wan, W., Zhang, C., and Zhang, W. (2018). MALAT1 promotes the colorectal cancer malignancy by increasing DCP1A expression and miR203 downregulation. Mol Carcinog *57*, 1421-1431. 10.1002/mc.22868.
Wu, D., Muhlrad, D., Bowler, M.W., Jiang, S., Liu, Z., Parker, R., and Song, H. (2014). Lsm2 and Lsm3 bridge the interaction of the Lsm1-7 complex with Pat1 for decapping activation. Cell Res *24*, 233-246. 10.1038/cr.2013.152.
Wu, H., Zhang, J., Bai, Y., Zhang, S., Zhang, Z., Tong, W., Han, P., Fu, B., Zhang, Y., and Shen, Z. (2021a). DCP1A is an unfavorable prognostic-related enhancer RNA in hepatocellular carcinoma. Aging (Albany NY) *13*, 23020-23035. 10.18632/aging.203593.
Wu, T., Hu, E., Xu, S., Chen, M., Guo, P., Dai, Z., Feng, T., Zhou, L., Tang, W., Zhan, L., et al. (2021b). clusterProfiler 4.0: A universal enrichment tool for interpreting omics data. Innovation (Camb) *2*, 100141. 10.1016/j.xinn.2021.100141.
Wurm, J.P., Holdermann, I., Overbeck, J.H., Mayer, P.H.O., and Sprangers, R. (2017). Changes in conformational equilibria regulate the activity of the Dcp2 decapping enzyme. Proc Natl Acad Sci U S A *114*, 6034-6039. 10.1073/pnas.1704496114.
Yi, H., Park, J., Ha, M., Lim, J., Chang, H., and Kim, V.N. (2018). PABP Cooperates with the CCR4-NOT Complex to Promote mRNA Deadenylation and Block Precocious Decay. Mol Cell *70*, 1081-1088 e1085. 10.1016/j.molcel.2018.05.009.

Figure legends

Figure 1 DCP1 is essential for human decapping process

(A) Wild-type or DCP1a/b knockout HEK-293T cells were transfected with a mixture of plasmids. One plasmid expressed the β-globin-6xMS2bs, another plasmid expressed the transfection control which contained the β-globin gene fused to the GAPDH 3' UTR, but it lacked the MS2 binding sites (β-globin-GAP, Control). The third plasmid expressed a MS2-HA or the MS2-tagged SMG7 proteins, and a fourth plasmid encoding a GFP-tagged protein was included in the transfection mixtures where indicated. A northern blot of representative RNA samples is shown. The positions of the polyadenylated (An) and the deadenylated (A_0) forms of the β-globin-6xMS2bs reporters are indicated on the right. A red dotted line additionally marks the fast migrating deadenylated (A_0) form. The DCP2 inactive mutant (E148Q) serves as a negative control. (B) Complementation assays with GFP-DCP1a or GFP-DCP1b constructs in HEK-293T DCP1a/b-null cells performed essentially as in panel (A). (C) The β-globin-6xMS2bs mRNA levels were normalized to those of the control mRNA. These normalized values were set to 100 in cells expressing MS2-HA (white bars). The mean values for relative mRNA levels in cells expressing MS2-SMG7 were estimated with standard deviations (SD) from three independent experiments (black bars). (D) A western blot demonstrating equivalent expression of the GFP-tagged proteins in panel (A) and (B). Tubulin served as a loading control. (E) The domain organization of human DCP1a. (F) Complementation assays with GFP-DCP1a deletion constructs in HEK-293T DCP1a/b-null cells performed essentially as in panel (A). (G) The β-globin-6xMS2bs mRNA levels were normalized to those of the control mRNA. These normalized values were set to 100 in cells expressing MS2-HA (white bars). The mean values for relative mRNA levels in cells expressing MS2-SMG7 were estimated with standard deviations (SD) from three independent experiments (black bars). (H) A western blot demonstrating equivalent expression of the GFP-tagged proteins in panel (F). Tubulin served as a loading control. (I) Complementation assays with GFP-DCP1a fragment constructs in HEK-293T DCP1a/b-null cells performed essentially as in panel (A). (J) The β-globin-6xMS2bs mRNA levels were normalized to those of the control mRNA. These normalized values were set to 100 in cells expressing MS2-HA (white bars). The mean values for relative mRNA levels in cells expressing MS2-SMG7 were estimated with standard deviations (SD) from three independent experiments (black bars). (K) A western blot demonstrating equivalent expression of the GFP-tagged proteins in panel (I). Tubulin served as a loading control.

Figure 2 DCP1 serves as a bridging factor facilitating the interaction between multiple decapping factors and DCP2.

(A) HEK-293T wild-type or DCP1a/b-null cells were stained with antibodies detecting DCP2 (red) and a P-body marker, EDC4 (green), then counterstained with DAPI to visualize the nucleus (blue). In the merged image, colocalization of DCP2 and EDC4 localization appears yellow. Scale bar=10 μm. (B) GFP-tagged DCP2 proteins were expressed in human HEK-293T wild-type or DCP1a/b-null cells. Subsequently, purification was performed using GFP antibody and IgG beads. *In vitro* decapping activity was then tested, with the catalytically inactive DCP2 E148Q mutant served as a negative control. (C) Decapping assays *in vitro*. The fraction of decapped mRNA substrate, measured by the release of m^7GDP (panel B), is plotted as a function of time. Error bars, standard deviations (SD) from three independent experiments. (D)

The GFP-DCP2 WT or E148Q immunoprecipitated samples corresponding to panel (B) were analyzed by Western blotting using the indicated antibodies. (E) V5-Streptavidin-Binding Peptide (SBP)-DCP2 proteins were expressed in human HEK-293T wild-type or DCP1a/b-null cells, followed by purification using Strepavidin beads. The interaction of V5-SBP-tagged DCP2 with endogenous decapping factors in wild-type or DCP1a/b knockout HEK-293T cells. Strepavidin resin was used for immunoprecipitate the V5-SBP-DCP2 in the presence of RNase A. Bound proteins were detected via Western blot. V5-SBP-MBP employed as a negative control. (F-G) The interaction of GFP-tagged DCP2 with HA-tagged PNRC1 (F) or V5-tagged PNRC2 (G). The proteins were immunoprecipitated using anti-GFP antibodies and analyzed by Western blotting using the indicated antibodies.

Figure 3 DCP1 facilitates DCP2 interactions with RNA molecules in human cells

(A-D) The interaction of GFP-tagged DCP2 with indicated decapping factors. The proteins were immunoprecipitated using anti-GFP antibodies and analyzed as described in Figure 2D and E. (E) The tethering assays with control, shPNRC1 or shPNRN2 plasmids in HEK-293T cells performed essentially as in Figure 1A. (F) The β-globin-6xMS2bs mRNA levels were normalized to those of the control mRNA. These normalized values were set to 100 in cells expressing MS2-HA (white bars). The mean values for relative mRNA levels in cells expressing MS2-SMG7 were estimated with standard deviations (SD) from three independent experiments (black bars). (G) Schematic representation of the experimental procedure in panel H and J. (H) DCP1a/b-null HEK-293T cells were transfected with a plasmid mixture containing the β-globin-6xMS2bs, MS2-HA-Strep-SMG7, V5-SBP-DCP2 E148Q, and either full-length or EVH1 domain of GFP-DCP1a. GFP-MBP serves as a control. The levels of β-globin-6xMS2bs mRNA bound to V5-SBP-DCP2 E148Q were then immunoprecipitated using streptavidin beads and quantified by RT-PCR with GAPDH as a reference. The results presented in each panel represent the mean values ± standard deviations (SD) of three biological replicates. (I) The V5-SBP-DCP2 E148Q immunoprecipitated samples corresponding to Figure 3H were analyzed by Western blotting using the indicated antibodies. (J) The plasmid mixture was transfected to DCP1a/b-null HEK-293T cells as detailed in panel H. Subsequently, Strep-tag beads were used to immunoprecipitate the MS2-HA-Strep-SMG7 bound β-globin-6xMS2bs mRNA to study the in vivo interaction levels between RNA molecules and DCP2 E148Q in the presence of GFP-DCP1a full-length or EVH1 domain. GFP-MBP serves as a control.

Figure 4 Gene expression analysis and pathway enrichment reveal distinct roles of DCP1a and DCP1b in human cells

(A) The upper and lower panels display Venn diagrams illustrating the number of genes that were significantly up- and down-regulated in DCP1a, DCP1b, and DCP1a/b knockout cells (referred to as DCP1a_KO, DCP1b_KO, and DCP1a/b_KO), respectively. The overlapping regions between the diagrams indicate the number of genes that were significantly altered in multiple cell lines. (B) The plot shows the distribution of fold changes in genes when comparing DCP1a_KO or DCP1b_KO to WT. The points on the plot are colored according to the fold changes observed when comparing DCP1a/b_KO to WT. GSEA results for the comparison of (C) hallmark and (D) KEGG pathways between DCP1a knockout and WT and DCP1b knockout

and WT. The left and right panels show activated and suppressed pathways, respectively. The dots were colored based on the q-value. (E) Boxplots of the mRNA expression levels of DCP1a and DCP1b in various cancer types in TCGA. Statistically significant differences in the expression levels were labeled on top of each pair (Wilcoxon test, *: p <= 0.05; **: p <= 0.01; ***: p <= 0.001; ****: p <= 0.0001).

Figure 5 Metabolome profiling unveils unique functions of DCP1 paralogs in human cells

(A) PLS-DA plot illustrating the metabolome profiles of the 12 samples, with 3 technical replicates for each knockout cell-line. Volcano plots for comparing metabolite levels of (B) DCP1a_KO and WT, (C) DCP1b_KO and WT, and (D) DCP1a/b_KO and WT. Metabolites with an absolute fold change greater than 1.5 and a false discovery rate (FDR)-adjusted p-value less than 0.01 were considered significant. The box plots of (E) UDP-GlcNAc and (F) GlcNAc between cell-lines. (G) Normalized expression levels/abundance of transcripts and metabolites, and the fold changes in amino sugar and nucleotide sugar metabolism pathway. Significantly upregulated and downregulated genes are colored in pink and blue, respectively. Upregulated and downregulated metabolites are colored in red and blue, respectively.

Supplemental Figures

Supplementary Figure S1

(A) The protein levels of DCP1a and DCP1b were quantified in HEK-293T wild-type (WT) cells and in DCP1a, DCP1b, and DCP1a/b-knockout cell lines (DCP1a KO, DCP1b KO, and DCP1a/b KO). Western blot analysis was performed on knockout cell clones to evaluate the expression of DCP1a and DCP1b, with tubulin serving as the loading control. (B) Sanger sequencing of the DCP1a/b genomic region targeted by the DCP1a/b sgRNAs in DCP1a/b knockout clone. Frameshift mutations were detected to generate premature STOP codons (PTC) in DCP1a/b of both alleles. (−: deleted bases; green: PAM sequence).

Supplementary Figure S2

(A) The tethering assays using the β-globin-6xMS2bs reporter were conducted similarly to the procedure described in Figure 1A, with the exception that MS2-SMG7 was replaced by either MS2-HA-TNRC6A silencing domain (TNRC6A-SD) or MS2-HA-Nanos1 (Nanos1), as indicated. MS2-HA-GFP serves as a control. (B) The graph shows the quantification of mRNA levels of the β-globin-6xMS2bs reporter normalized to the levels of the control reporter and set to 100 for MS2-HA-GFP; the mean values ± standard deviations (SD) are shown for three independent experiments. (C) Representative Western blot depicting the equivalent expression of the MS2-HA-tagged proteins used in (A). Tubulin served as a loading control. (D) The RNA samples from Figure 1A were incubated in the absence or presence of Terminator 5'-phosphatedependent

exonuclease and analyzed by northern blotting. 28S and 18S ribosomal RNA served as uncapped control.

Supplementary Figure S3

HEK-293T cells of both the wild-type and DCP1a/b-null types were subjected to staining using antibodies that detect DCP2 (red) as well as P-body markers (green), 4E-T (A) or DDX6 (B). The stained cells were then counterstained using DAPI, which allows the visualization of the nucleus (blue). Scale bar=10 μm.

Supplementary Figure S4

HEK-293T cells were transfected with shRNA plasmid sequences targeting PNRC1 or PNRC2 to induce RNAi-mediated silencing. As a negative control, cells were also transfected with a non-targeting shRNA. Protein levels of PNRC1 (A) and PNRC2 (B) were subsequently detected using western blot analysis.

Supplementary Figure S5

(A) PCA plot showing the transcriptome profiles of 12 samples including wild-type HEK-293T and DCP1 knockout cell lines (DCP1a_KO, DCP1b_KO, and DCP1a/b_KO). Volcano plots for comparing transcript levels of (B) DCP1a knockout and the wild-type, (C) DCP1b knockout and the wild-type, and (D) DCP1a/b double knockout and the wild-type.Genes that show a significant increase are marked in pink (fold change > 1.5, adjusted p value < 0.05), while genes that show a significant decrease are marked in green (fold change < -1.5, adjusted p value < 0.05). GSEA results for comparison of biological process GO terms (E), cellular component GO terms (F), molecular function GO terms (G), and Reactome pathways (H) between DCP1a knock out and WT, and DCP1b knock out and WT. Left and right panels show activated and suppressed pathways, respectively.

Supplementary Figure S6

The (A) PLS-DA loading plot and (B) heatmap of the top 25 features with the highest VIP scores from DCP1a_KO, DCP1b_KO, DCP1a/b_KO, and WT cell-lines. The box plots of (C) glycerophosphocholine, (D) glycerophosphoserine, (E) NAD and (F) LPE(P-18:0) between wild-type and DCP1 knockout cell-lines.

Supplementary Figure S7

Amino sugar and nucleotide sugar metabolism pathways colored based on the fold change of transcript (green and red) or metabolites (blue and yellow) in an order of DCP1a_KO to WT, DCP1a/b_KO to WT and DCP1b_KO to WT.

Fig.1

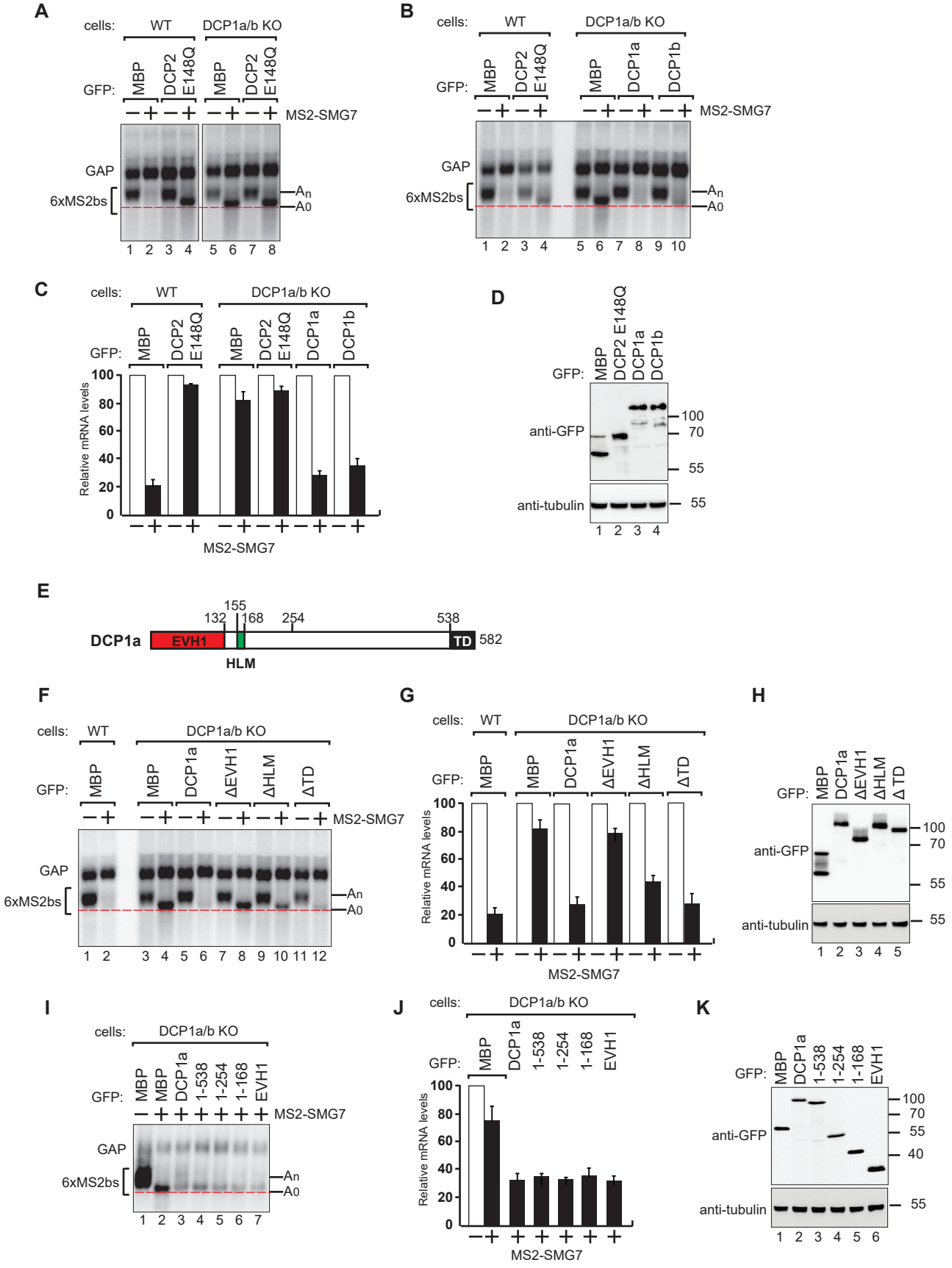
A
cells: WT DCP1a/b KO
GFP: MBP DCP2 E148Q MBP DCP2 E148Q
MS2-SMG7
GAP
6xMS2bs
An
A0
1 2 3 4 5 6 7 8
B
cells: WT DCP1a/b KO
GFP: MBP DCP2 E148Q MBP DCP1a DCP1b
MS2-SMG7
GAP
6xMS2bs
An
A0
1 2 3 4 5 6 7 8 9 10
C
cells: WT DCP1a/b KO
GFP: MBP DCP2 E148Q MBP DCP2 E148Q DCP1a DCP1b
Relative mRNA levels
100 80 60 40 20 0
MS2-SMG7
D
GFP: MBP DCP2 E148Q DCP1a DCP1b
anti-GFP
anti-tubulin
100 70 55 55
1 2 3 4
E
DCP1a
EVH1
HLM
TD
132 155 168 254 538 582
F
cells: WT DCP1a/b KO
GFP: MBP MBP DCP1a ΔEVH1 ΔHLM ΔTD
MS2-SMG7
GAP
6xMS2bs
An
A0
1 2 3 4 5 6 7 8 9 10 11 12
G
cells: WT DCP1a/b KO
GFP: MBP MBP DCP1a ΔEVH1 ΔHLM ΔTD
Relative mRNA levels
100 80 60 40 20 0
MS2-SMG7
H
GFP: MBP DCP1a ΔEVH1 ΔHLM Δ TD
anti-GFP
anti-tubulin
100 70 55 55
1 2 3 4 5
I
cells: DCP1a/b KO
GFP: MBP MBP DCP1a 1-538 1-254 1-168 EVH1
MS2-SMG7
GAP
6xMS2bs
An
A0
1 2 3 4 5 6 7
J
cells: DCP1a/b KO
GFP: MBP DCP1a 1-538 1-254 1-168 EVH1
Relative mRNA levels
100 80 60 40 20 0
MS2-SMG7
K
GFP: MBP DCP1a 1-538 1-254 1-168 EVH1
anti-GFP
anti-tubulin
100 70 55 40 55
1 2 3 4 5 6

Fig.2

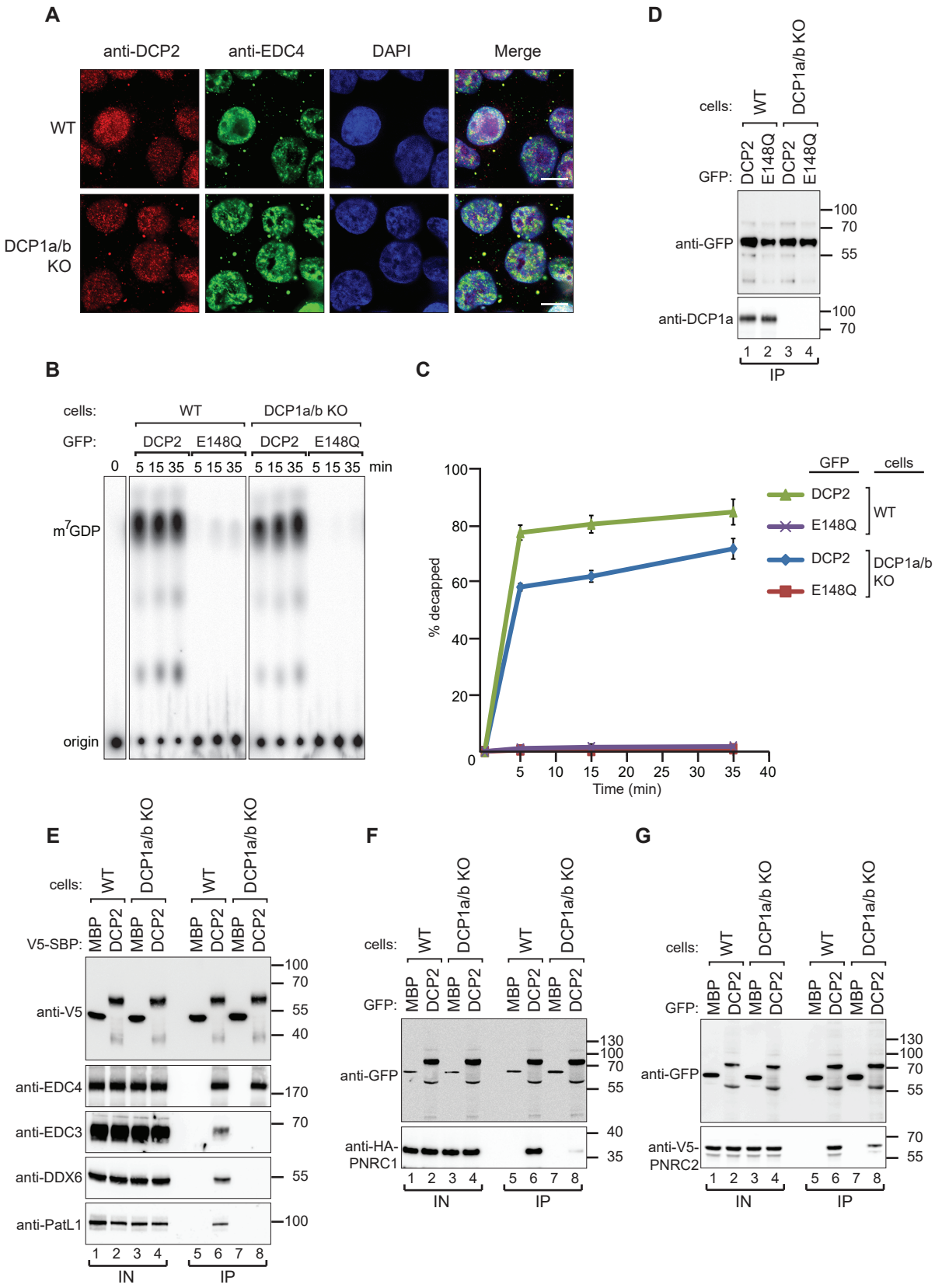
A
anti-DCP2
anti-EDC4
DAPI
Merge
WT
DCP1a/b KO
B
cells:
WT
DCP1a/b KO
GFP:
DCP2
E148Q
DCP2
E148Q
0
5 15 35
5 15 35
5 15 35
5 15 35
min
m7GDP
origin
C
% decapped
Time (min)
GFP
cells
DCP2
E148Q
WT
DCP2
E148Q
DCP1a/b KO
D
cells:
WT
DCP1a/b KO
GFP:
DCP2
E148Q
DCP2
E148Q
anti-GFP
anti-DCP1a
IP
E
cells:
WT
DCP1a/b KO
V5-SBP:
MBP
DCP2
anti-V5
anti-EDC4
anti-EDC3
anti-DDX6
anti-PatL1
IN
IP
F
cells:
WT
DCP1a/b KO
GFP:
MBP
DCP2
anti-GFP
anti-HA-PNRC1
IN
IP
G
cells:
WT
DCP1a/b KO
GFP:
MBP
DCP2
anti-GFP
anti-V5-PNRC2
IN
IP

Fig.3

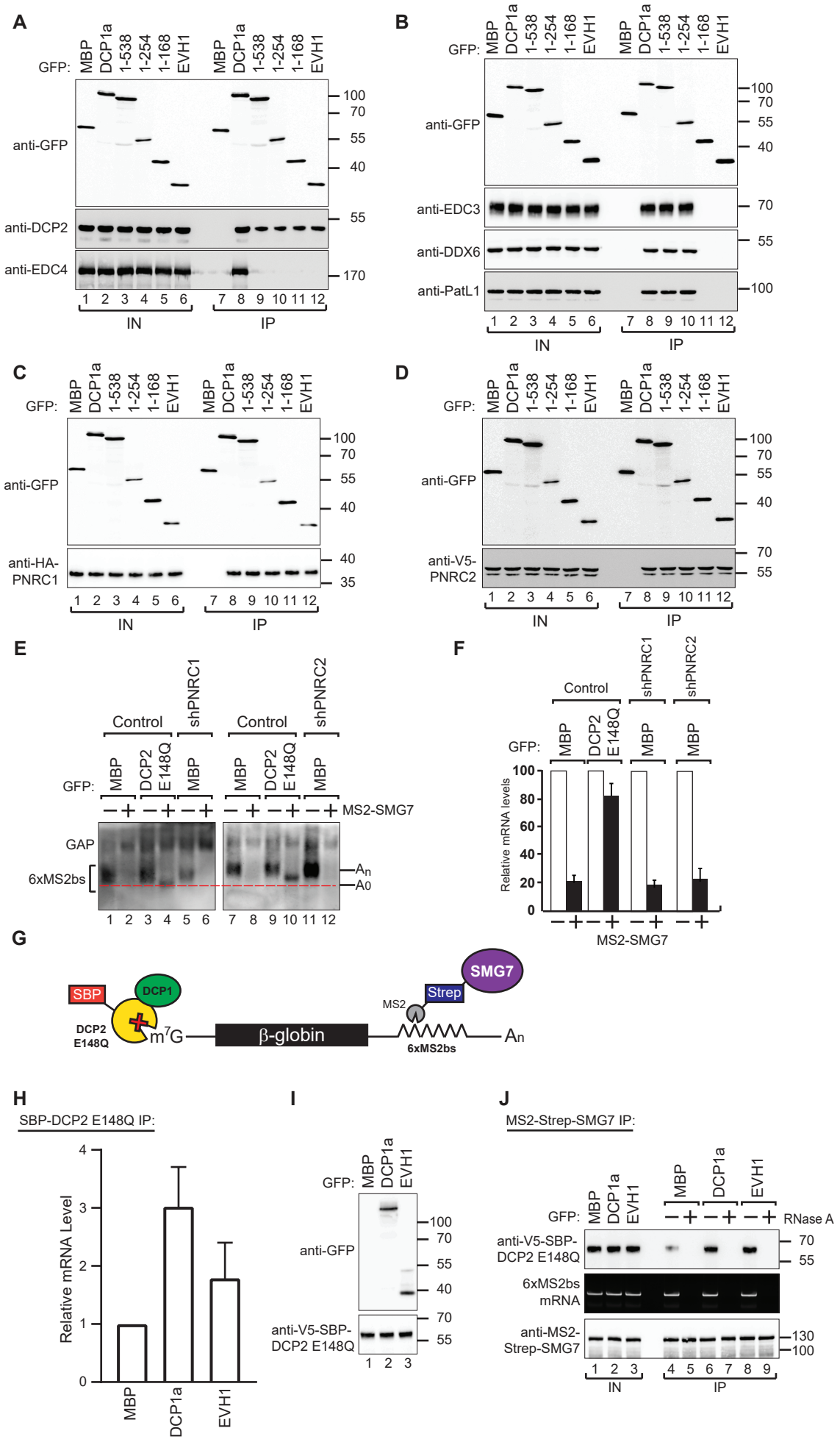
A
GFP:
MBP
DCP1a
1-538
1-254
1-168
EVH1
anti-GFP
anti-DCP2
anti-EDC4
100
70
55
40
170
IN
IP
B
anti-EDC3
anti-DDX6
anti-PatL1
C
anti-HA-PNRC1
35
D
anti-V5-PNRC2
E
Control
shPNRC1
shPNRC2
DCP2 E148Q
MS2-SMG7
GAP
6xMS2bs
An
A0
F
Relative mRNA levels
G
SBP
DCP1
DCP2 E148Q
m7G
β-globin
MS2
Strep
SMG7
6xMS2bs
H
SBP-DCP2 E148Q IP:
Relative mRNA Level
I
J
MS2-Strep-SMG7 IP:
RNase A
anti-V5-SBP-DCP2 E148Q
6xMS2bs mRNA
anti-MS2-Strep-SMG7
130

Fig.4

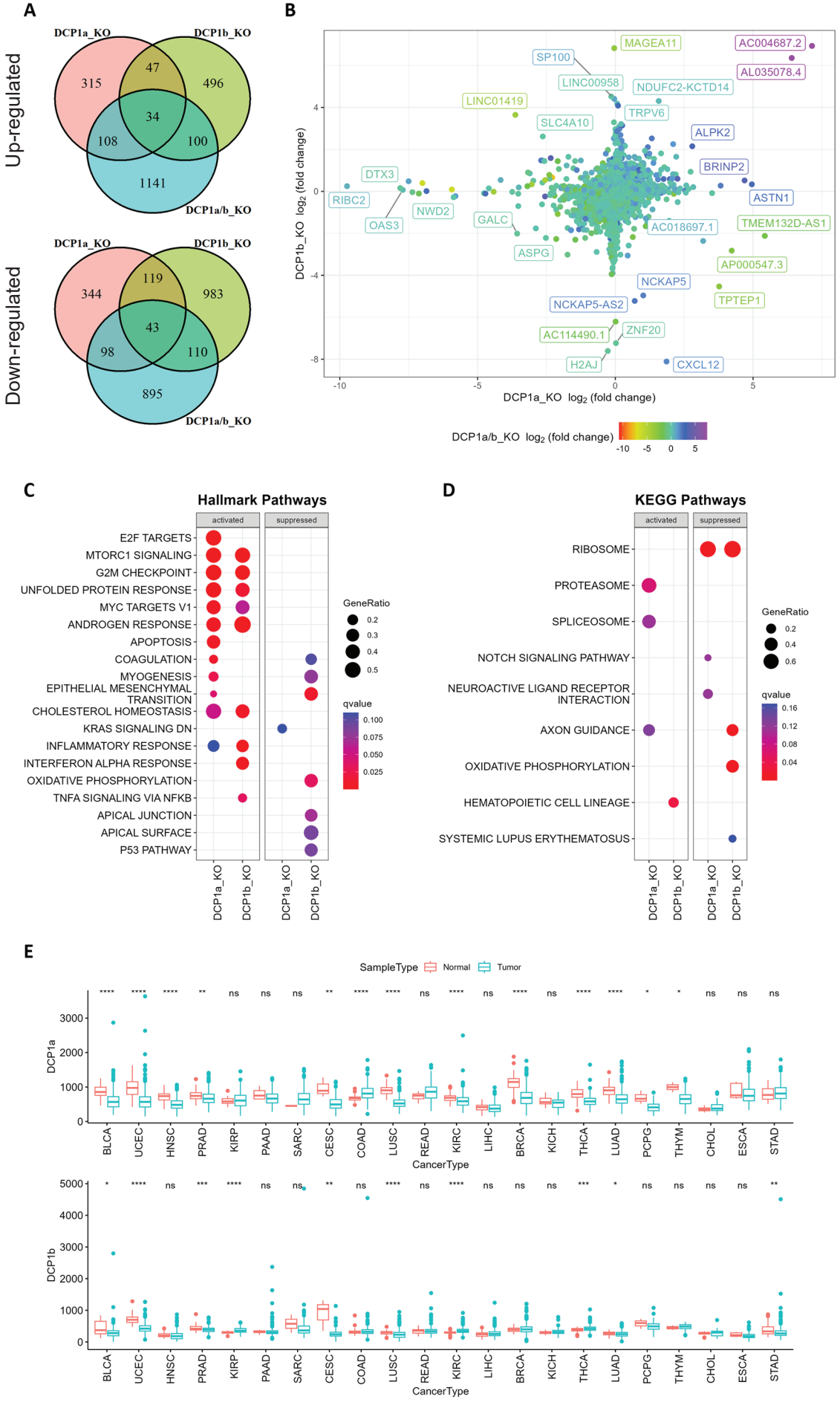
A
Up-regulated
DCP1a_KO
DCP1b_KO
DCP1a/b_KO
315
47
496
34
108
100
1141
Down-regulated
344
119
983
43
98
110
895
B
DCP1b_KO log2 (fold change)
DCP1a_KO log2 (fold change)
DCP1a/b_KO log2 (fold change)
MAGEA11
AC004687.2
AL035078.4
SP100
LINC00958
NDUFC2-KCTD14
LINC01419
TRPV6
SLC4A10
ALPK2
BRINP2
DTX3
RIBC2
ASTN1
NWD2
OAS3
GALC
AC018697.1
TMEM132D-AS1
ASPG
AP000547.3
NCKAP5
TPTEP1
NCKAP5-AS2
AC114490.1
ZNF20
H2AJ
CXCL12
C
Hallmark Pathways
activated
suppressed
E2F TARGETS
MTORC1 SIGNALING
G2M CHECKPOINT
UNFOLDED PROTEIN RESPONSE
MYC TARGETS V1
ANDROGEN RESPONSE
APOPTOSIS
COAGULATION
MYOGENESIS
EPITHELIAL MESENCHYMAL TRANSITION
CHOLESTEROL HOMEOSTASIS
KRAS SIGNALING DN
INFLAMMATORY RESPONSE
INTERFERON ALPHA RESPONSE
OXIDATIVE PHOSPHORYLATION
TNFA SIGNALING VIA NFKB
APICAL JUNCTION
APICAL SURFACE
P53 PATHWAY
GeneRatio
qvalue
D
KEGG Pathways
RIBOSOME
PROTEASOME
SPLICEOSOME
NOTCH SIGNALING PATHWAY
NEUROACTIVE LIGAND RECEPTOR INTERACTION
AXON GUIDANCE
OXIDATIVE PHOSPHORYLATION
HEMATOPOIETIC CELL LINEAGE
SYSTEMIC LUPUS ERYTHEMATOSUS
E
SampleType
Normal
Tumor
DCP1a
DCP1b
CancerType
BLCA
UCEC
HNSC
PRAD
KIRP
PAAD
SARC
CESC
COAD
LUSC
READ
KIRC
LIHC
BRCA
KICH
THCA
LUAD
PCPG
THYM
CHOL
ESCA
STAD

Fig.5

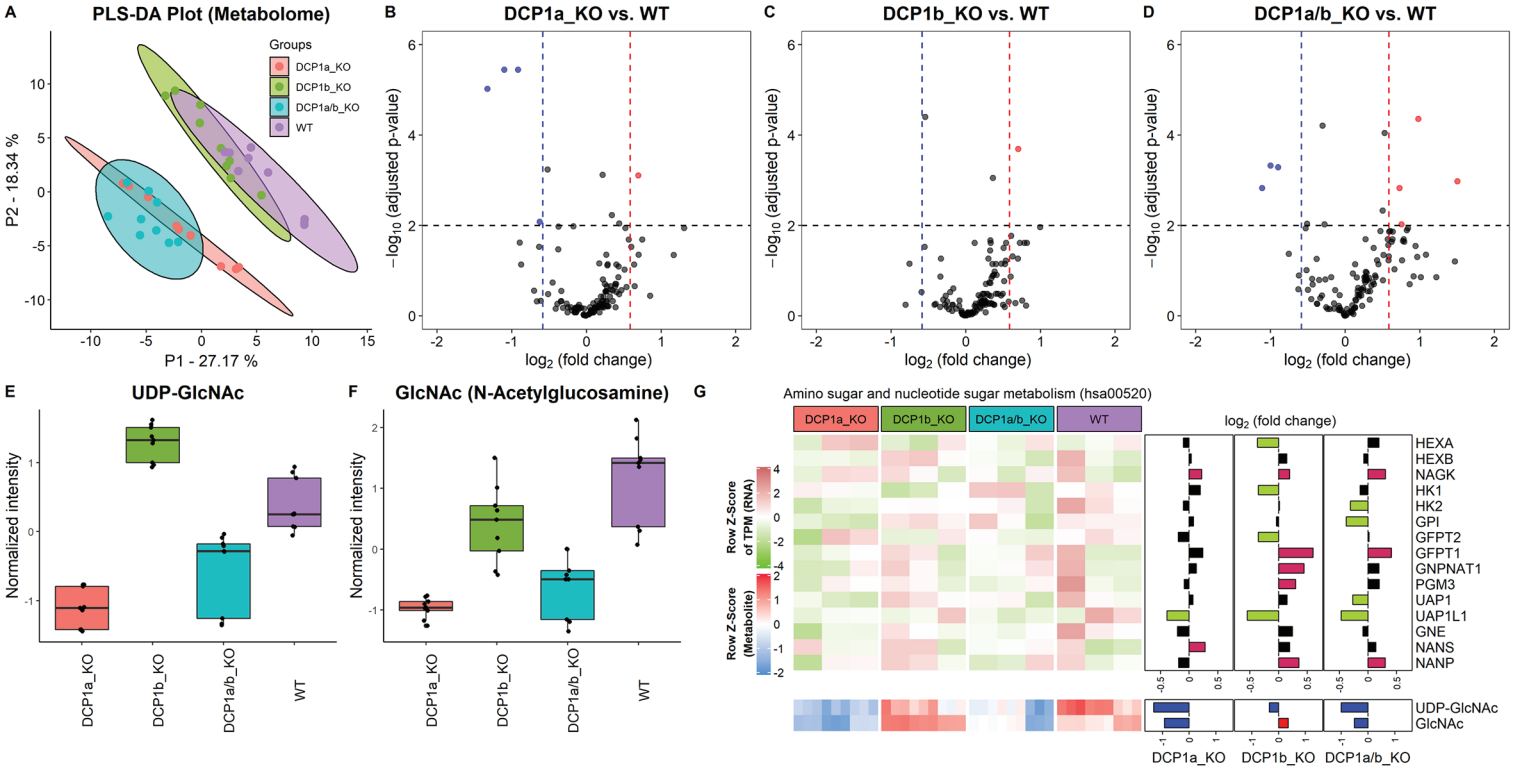
A
PLS-DA Plot (Metabolome)
Groups
DCP1a_KO
DCP1b_KO
DCP1a/b_KO
WT
P2 - 18.34 %
P1 - 27.17 %
B
DCP1a_KO vs. WT
C
DCP1b_KO vs. WT
D
DCP1a/b_KO vs. WT
−log10 (adjusted p-value)
log2 (fold change)
E
UDP-GlcNAc
F
GlcNAc (N-Acetylglucosamine)
Normalized intensity
G
Amino sugar and nucleotide sugar metabolism (hsa00520)
Row Z-Score of TPM (RNA)
Row Z-Score (Metabolite)
log2 (fold change)
HEXA
HEXB
NAGK
HK1
HK2
GPI
GFPT2
GFPT1
GNPNAT1
PGM3
UAP1
UAP1L1
GNE
NANS
NANP
UDP-GlcNAc
GlcNAc